AD-A077 194 GENERAL ELECTRIC CO SANTA BARBARA CA TEMPO F/G 14/2
DEVELOPMENT OF PASSIVE HIGH PRESSURE GAUGES - FIELD EXPERIMENT.(U)
JAN 79 J E SCHOUTENS , C C HUDSON DNA001-78-C-0285
UNCLASSIFIED GE78TMP-102 DNA-4768F NL

1 OF 1
AD A077194

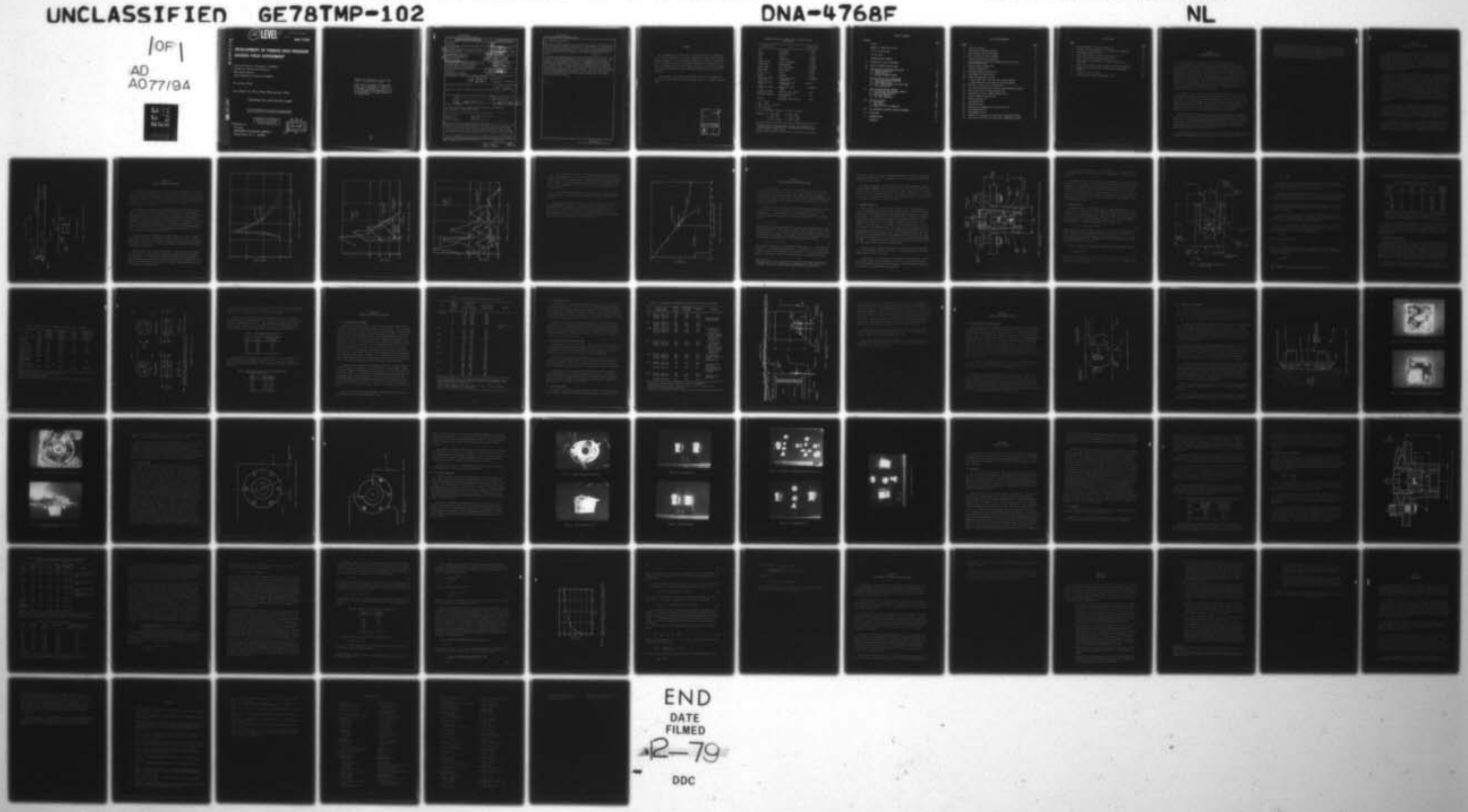

END
DATE FILMED
2-79
DDC

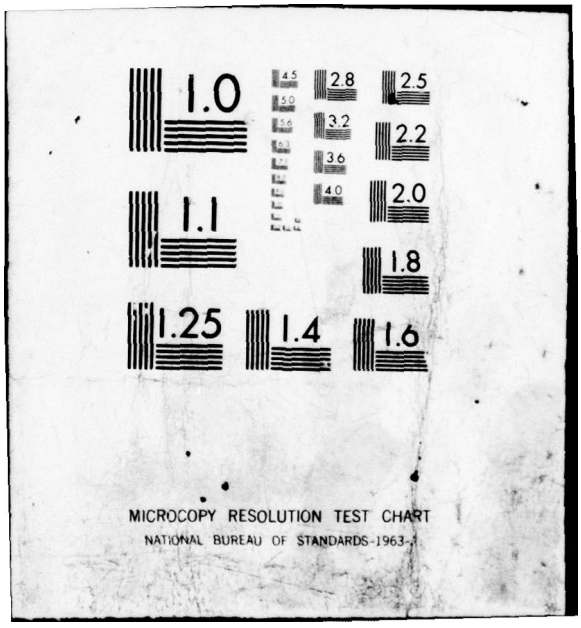
1.0
1.1
1.25
1.4
1.6
1.8
2.0
2.2
2.5
2.8
3.2
3.6
4.0
4.5
5.0
5.6
MICROCOPY RESOLUTION TEST CHART
NATIONAL BUREAU OF STANDARDS-1963-A

(12) LEVEL III

AD-E300 614

DNA 4768F

DEVELOPMENT OF PASSIVE HIGH PRESSURE GAUGES—FIELD EXPERIMENT

General Electric Company—TEMPO
Center for Advanced Studies
816 State Street
Santa Barbara, California 93102

31 January 1979

Final Report for Period May 1978—January 1979

CONTRACT No. DNA 001-78-C-0285

THIS WORK SPONSORED BY THE DEFENSE NUCLEAR AGENCY
UNDER RDT&E RMSS CODE B344078462 J11AAXSX35258 H2590D.

Prepared for
Director
DEFENSE NUCLEAR AGENCY
Washington, D. C. 20305

Destroy this report when it is no longer needed. Do not return to sender.

PLEASE NOTIFY THE DEFENSE NUCLEAR AGENCY, ATTN: STTI, WASHINGTON, D.C. 20305, IF YOUR ADDRESS IS INCORRECT, IF YOU WISH TO BE DELETED FROM THE DISTRIBUTION LIST, OR IF THE ADDRESSEE IS NO LONGER EMPLOYED BY YOUR ORGANIZATION.

UNCLASSIFIED

SECURITY CLASSIFICATION OF THIS PAGE (When Data Entered)

REPORT DOCUMENTATION PAGE

READ INSTRUCTIONS BEFORE COMPLETING FORM

1. REPORT NUMBER: DNA 4768F
2. GOVT ACCESSION NO.:
3. RECIPIENT'S CATALOG NUMBER: 9

4. TITLE (and Subtitle): DEVELOPMENT OF PASSIVE HIGH PRESSURE GAUGES—FIELD EXPERIMENT
5. TYPE OF REPORT & PERIOD COVERED: Final Report for Period May 78—Jan 79
6. PERFORMING ORG. REPORT NUMBER: GE78TMP-102

7. AUTHOR(s): Jacques E. Schoutens, Craig C. Hudson, Steven L. Senesac
8. CONTRACT OR GRANT NUMBER(s): DNA 001-78-C-0285

9. PERFORMING ORGANIZATION NAME AND ADDRESS: General Electric Company—TEMPO, Center for Advanced Studies, 816 State Street, Santa Barbara, California 93102
10. PROGRAM ELEMENT, PROJECT, TASK AREA & WORK UNIT NUMBERS: Subtask J11AAXSX352-58

11. CONTROLLING OFFICE NAME AND ADDRESS: Director, Defense Nuclear Agency, Washington, D.C. 20305
12. REPORT DATE: 31 January 1979
13. NUMBER OF PAGES: 74

14. MONITORING AGENCY NAME & ADDRESS (if different from Controlling Office)
15. SECURITY CLASS (of this report): UNCLASSIFIED
15a. DECLASSIFICATION/DOWNGRADING SCHEDULE

16. DISTRIBUTION STATEMENT (of this Report)

Approved for public release; distribution unlimited.

17. DISTRIBUTION STATEMENT (of the abstract entered in Block 20, if different from Report)

18. SUPPLEMENTARY NOTES

This work sponsored by the Defense Nuclear Agency under RDT&E RMSS Code B344078462 J11AAXSX35258 H2590D.

19. KEY WORDS (Continue on reverse side if necessary and identify by block number)

High Pressure	T-5A Yuma, AZ field test
Passive	AFWL T-5A
Shock measurement	Metal Oxide Varistor

RbCl

20. ABSTRACT (Continue on reverse side if necessary and identify by block number)

High pressure passive gauges capable of measuring peak shock pressures in the range of 2 to 25 kbar near detonating high explosives are being developed. The operation of these gauges is based upon the characteristics of second order transformations in pure metals or single crystals of alkaline halides and changes in the electrical characteristics of metal oxide varistors (MOV).

This paper describes the results of an experiment in which three RbCl samples and four ZnO MOVs were placed against a 0.70-m thick concrete wall at the

DD FORM 1 JAN 73 1473 EDITION OF 1 NOV 65 IS OBSOLETE

UNCLASSIFIED

SECURITY CLASSIFICATION OF THIS PAGE (When Data Entered)

346 420

20. ABSTRACT (Continued)

other side of which 2570 kg of explosives were detonated. The explosive and the concrete wall formed the driver end of a large shock tube. The tube and back of the wall were covered over with alluvium. At the gauge location, the alluvium depth was approximately 5 m. The samples were each located inside an individual pressure cell assembled into groups on steel plates to form gauges.

The gauges were recovered some 2.5 m away from their original position. They had been translated and tumbled horizontally away from the burst point. The pressure cells were deformed and five out of seven samples were recovered--two MOVs and three RbCl. An examination of the RbCl samples indicated no phase change, meaning that the shock pressure appeared not to have reached the expected 12 kbar. The MOV samples were deformed, making the results of their reading of low confidence. Nevertheless, a tentative lower bound on the shock peak pressure can be placed at 9 kbar. The pressure cells suffered severe permanent deformation, leading to the conclusion that the dynamic stresses developed during their motion away from the burst point reached approximately 9 to 13 kbar.

PREFACE

We are indebted to Mr. Robert Bass of Sandia Laboratories, Albuquerque, NM for his kind assistance in providing computational support with the CHART D computer program. We are also grateful to Captain Dave Ray, Mr. Joe Renick, and Mr. Joe Ayala of the Air Force Weapons Laboratories, Kirtland AFB, NM for their encouragement and assistance during this project, and for the invaluable assistance received from Mr. Charles Bryant, also of AFWL, during the field operations.

The assistance and cooperation of our COR, first Mr. T.E. Kennedy and later Mr. R.C. Webb, both of the Defense Nuclear Agency, is gratefully acknowledged.

Summary of Conversion Factors (U.S. to metric units) and Prefixes

To Convert From	To	Multiply By
mils	millimeters	0.0254
inches	centimeters	2.54
feet	meters	0.3048
miles	kilometers	1.6093
square inches	square centimeters	6.4516
square feet	square meters	0.0929
cubic inches	cubic centimeters	16.38706
cubic feet	cubic meters	0.0283
gallons (U.S.)	liters	28.349
pounds	kilograms	0.454
pounds per square inch, psi	newtons per square centimeter	0.6894757
pounds per cubic inch	kilograms per cubic centimeter	27,679.90
pounds per square foot	newtons per square meter	47.88026
inches per second	centimeters per second	2.54
Fahrenheit degrees	Celsius degrees or Kelvins[a]	5/9
kilotons	terajoules (10^{12} Joules)	4.183

1 Pa = 1 N/m^2

1 Bar = 10^5 Pa = 14.5 psi

1 psi = 6.9 KPa

1 g = acceleration of gravity = 32 F/S^2 = 9.8 m/s^2

Prefixes: G = 10^9 = giga M = 10^6 = mega
K = 10^3 = kilo c = 10^{-2} = centi
μ = 10^{-6} = micro n = 10^{-9} = nano

[a]To obtain Celsius (C) temperature readings from Fahrenheit (F) readings, use C = (5/9) (F - 32). To obtain Kelvin (K) readings, use K = (5/9) (F - 32) + 273.15.

TABLE OF CONTENTS

LIST OF ILLUSTRATIONS

LIST OF TABLES

SECTION I
INTRODUCTION AND SUMMARY

This report presents a description of a field experiment in which seven passive high pressure cells were installed for the measurement of shock peak pressures produced by high explosives. The experiment was intended not only to test prototype pressure cell design configurations but also to provide shock peak pressure measurements in support of soil stress and equation of state calculations. The shock peak pressure to be measured was 12 kbar using pressure cells so designed as to record values over a range of 3 to 15 kbar. These measurements were designed to use three different solid state elements: metal oxide varistors (GE-MOV®) for pressures in the range of 3 to 9 kbar; rubidium chloride (RbCl) for pressures in the range of 4.5 to 7.5 kbar; and pure bismuth for pressures of 12 kbar. Pressure cells in groups of four were assembled on steel plates to form gauges.

The gauges and one bismuth cell were intended to be installed in the Air Force Weapons Laboratory (AFWL) T-5A field test to be conducted at Yuma, AZ. The test date was October 6, 1978 at which time we had installed behind the driver wall of T-5A one gauge containing four MOV elements and one gauge containing three RbCl elements. The remaining RbCl cell and the bismuth cell were not installed for reasons given below. This field experiment is part of a continuing program for the development of high pressure gauges to be used in high pressure and high displacement regions.

The first half of this report describes the field experiment, the calculational method used to determine the location of the gauges to measure pressures of interest, the pressure cell and gauge design configuration tested, their calibration, and field installation. The second half of this report discusses the gauge recovery and post-mortem analysis as well as an analysis of the results obtained. Conclusions and recommendations are given at the end of the report.

We had also used T-5A as a test bed to test the survivability of a small electronic package installed behind and against the driver wall. This package is part of an

in-house program to design and develop an active self-contained system to measure pressures or accelerations or velocities or displacements in regions near explosives where such parameters are large. Although this experiment was not supported under this contract, the results we believe may be of interest to the reader. Therefore, a brief description of the results is presented in Section VIII.

2

SECTION II
DESCRIPTION OF FIELD EXPERIMENT

The Air Force Weapons Laboratory conducted a trench test called T-5A in Yuma, AZ. Initially scheduled for late October 1978, the test schedule was advanced with a firing target date of October 6, 1978. Because the GE-TEMPO passive high pressure gauges could provide an additional means of measuring peak pressures on future field tests, these measurements were fielded as a developmental instrumentation project. These gauges were fielded on a non-interference basis due to the accelerated construction schedule (Reference 1).

Figure 1 shows a diagram of the trench cross section. It consisted of a long tunnel closed off at both ends by concrete walls. Somewhere along the mid-distance in the tunnel, a concrete plug was installed. The end shown in Figure 1 consisted of a concrete wall 2 feet thick and 12 feet by 12 feet in plan. The wall on the inside of the tunnel supported an explosive charge, initially planned as TNT, consisting of 20 percent TNT with 60 percent ANFO and 20 percent of another mixture. This charge had a density of 1.45 gm/cm^3 (according to AFWL, may have been 1.3 gm/cm^3) with a total weight of 5670 pounds and an effective thickness of 9 inches. It is important to note here that the charge had less energy than we had initially assumed to be the case on the basis of TNT with an effective thickness of 5 inches.

Also shown in Figure 1 is a HEST cavity consisting of five layers of primacord and situated somewhere between the driver wall supporting the explosive and the plug. As shown in Figure 1, our instrumentation package was installed near the base of the driver wall and on the opposite side of the charge. After installation, the backfill was emplaced in a configuration shown in Figure 1.

It is also worth noting here, in view of subsequent events, that the driver wall was expected to hold against the blast, much as did the driver wall in the preceeding T-3 event. This means that our instrumentation package was not expected to undergo more than a few tens of centimeter horizontal displacement.

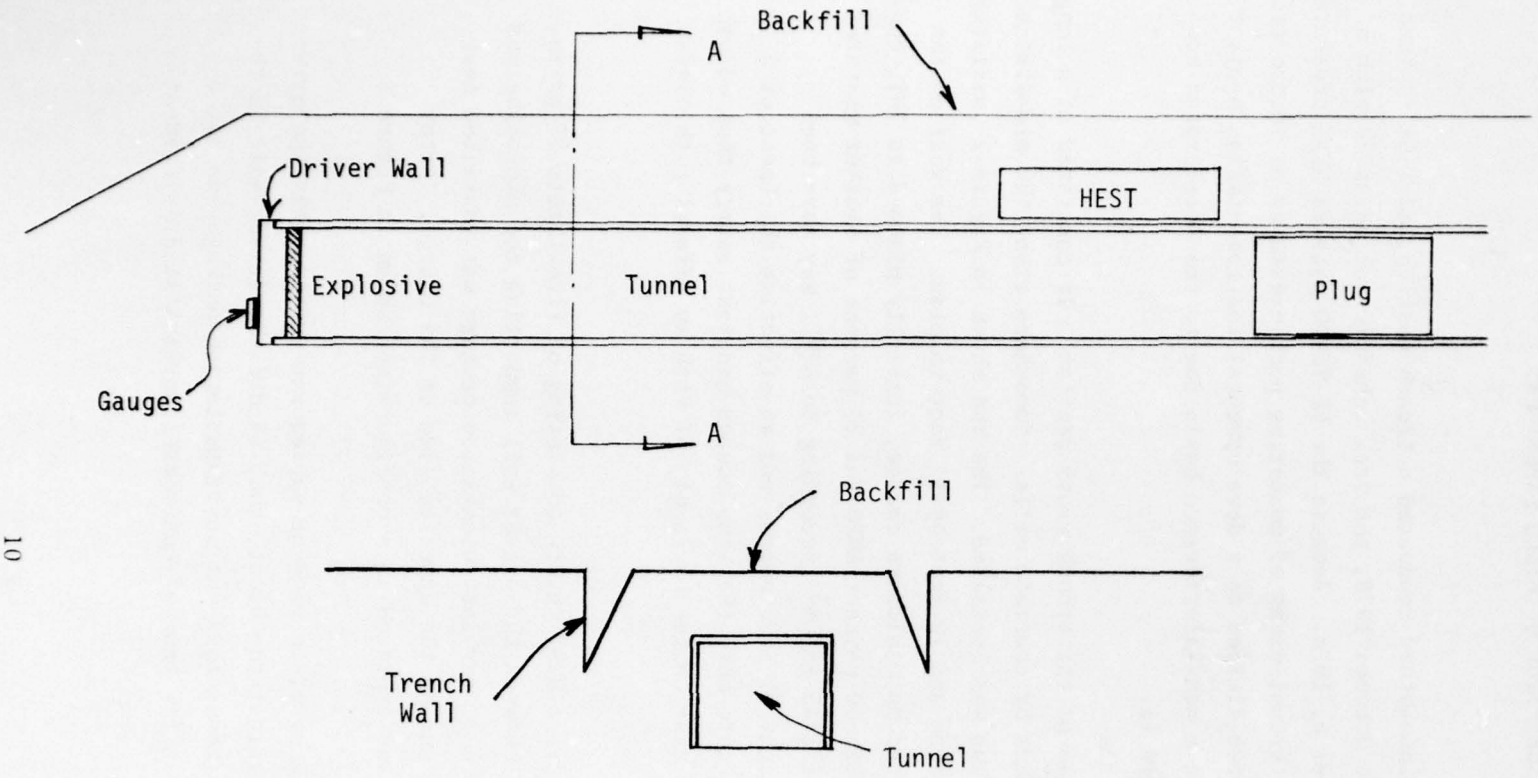

Trench Cross Section A-A

Figure 1. T-5A cross section (No Scale).

SECTION III
CHART D HYDROCODE CALCULATIONS

In order to determine where best to locate the gauges, we resorted to calculations kindly supplied GE-TEMPO by Robert Bass at Sandia (Reference 2). The computer code used is CHART D developed at Sandia Laboratories some years ago to perform one-dimensional hydrodynamic calculations in various media. It has been used extensively in the past to test equations of state for NTS environment and results have been generally excellent (Reference 2).

The problem run was based on the assumption that 5 inches of TNT would be used with a driver wall 27.5 inches in thickness. The driver wall was assumed to be backed by an infinite slab of alluvium or tuff. The equation of state of TNT used is not exactly correct for the explosive intended, but represented a good enough approximation. The equation of state for wet tuff was used for the concrete, as it was found to represent concrete well enough for our purposes. The equation of state of alluvium was developed by Bass (Reference 2) and represents other known data quite well. As will be shown below, the alluvium equation of state gives rise to very much more wave structure that does the dry tuff.

Results of these two calculations are shown in Figures 2, 3, and 4. Figure 2 shows the pressure pulse at the interface between the back of the driver wall and the backfill. There is most certainly some structure to these pulses, but the printout does not give the details. The plots represent results obtained from pressures calculated for a single zone.

Figures 3 and 4 show the pressure waveforms at different times versus distance into the backfill. These plots were obtained from a number of zones at different time intervals. One can clearly see the complex behavior of the alluvium model. The dry tuff shows the simple precursor wave. Other calculations (Reference 2) confirm that at lower pressures, the dry tuff wave exhibits the same structure as seen here for alluvium at high pressures.

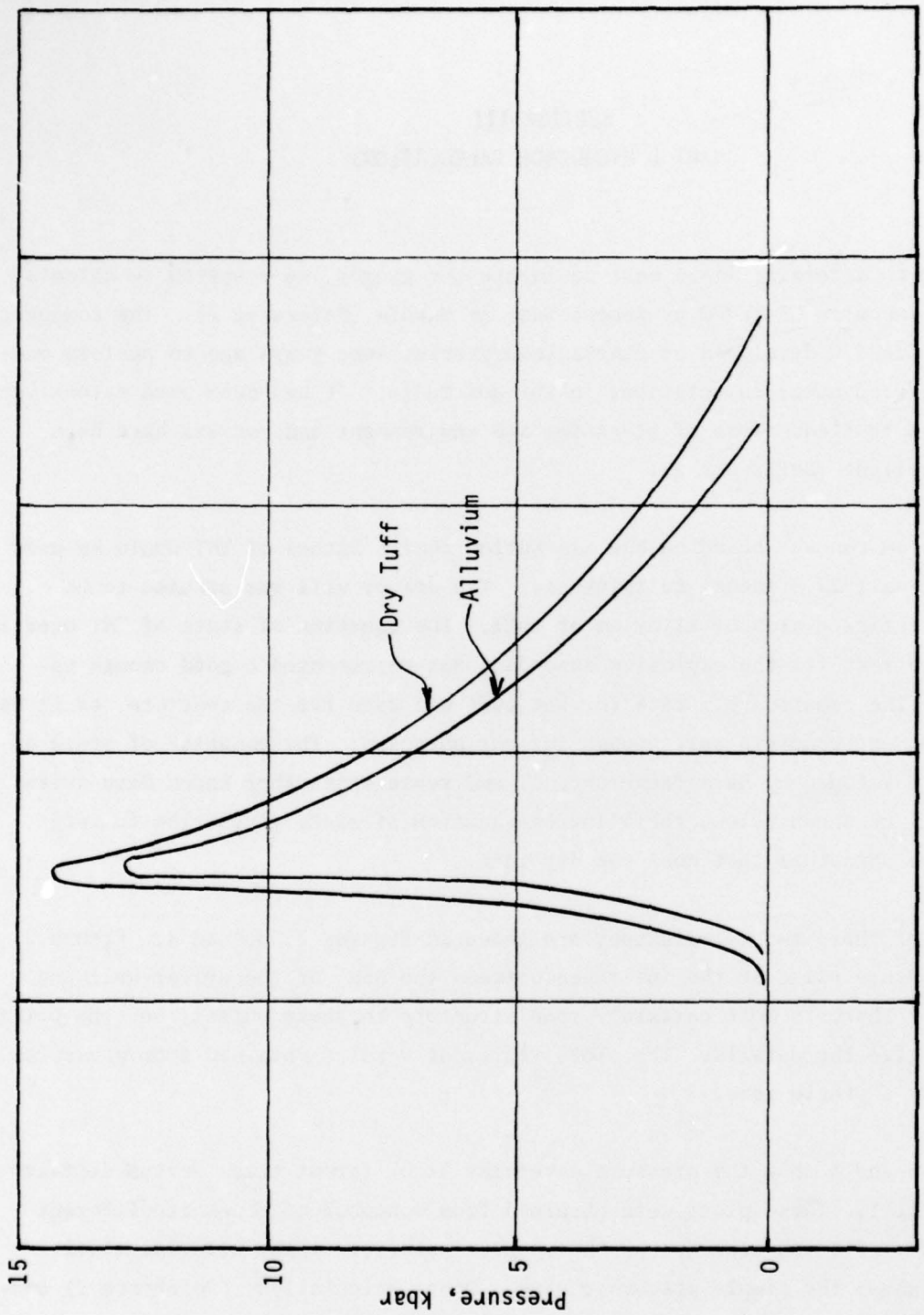

Figure 2. Concrete/soil interface pressure.

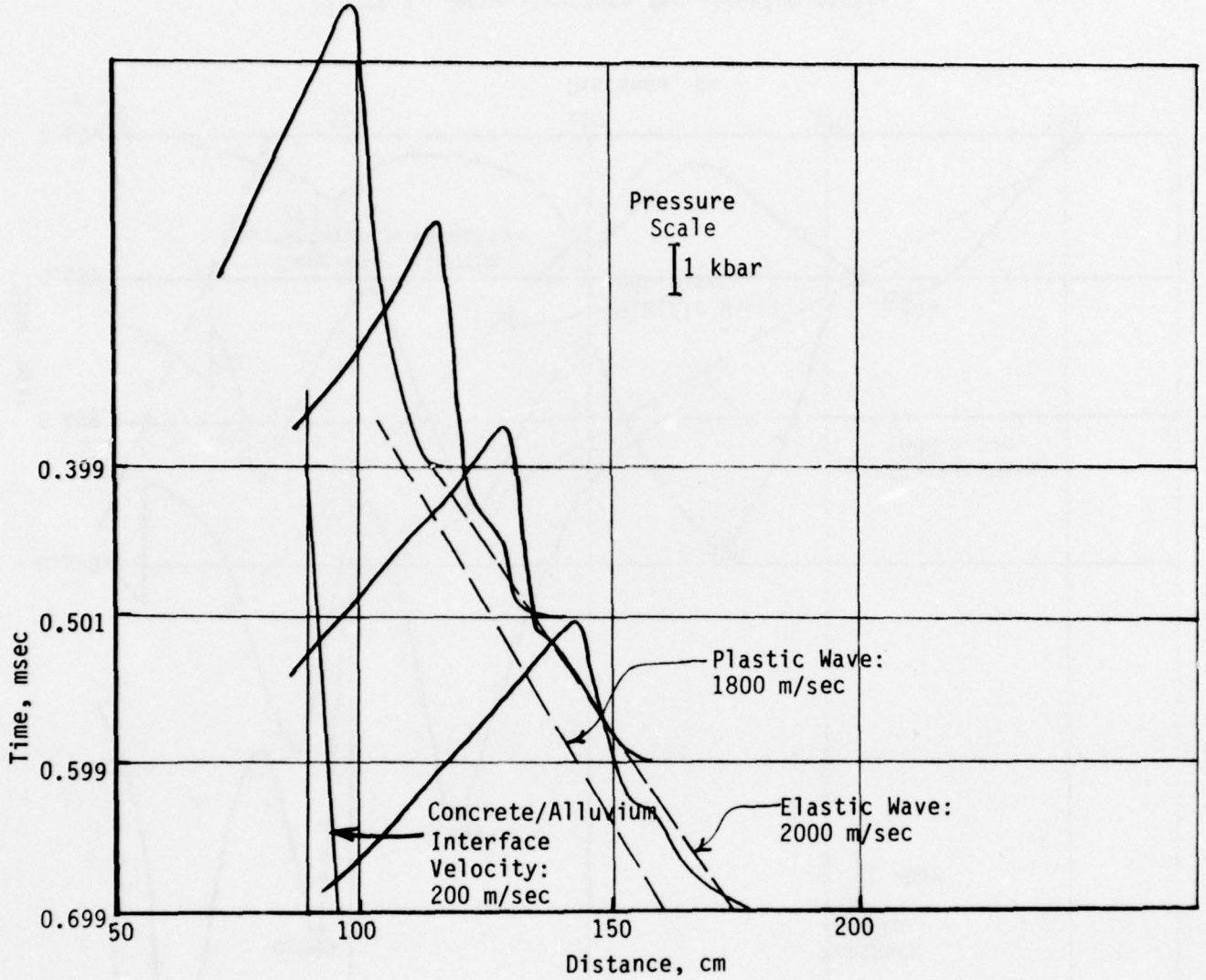

Figure 3. Wave structure for dry tuff model.

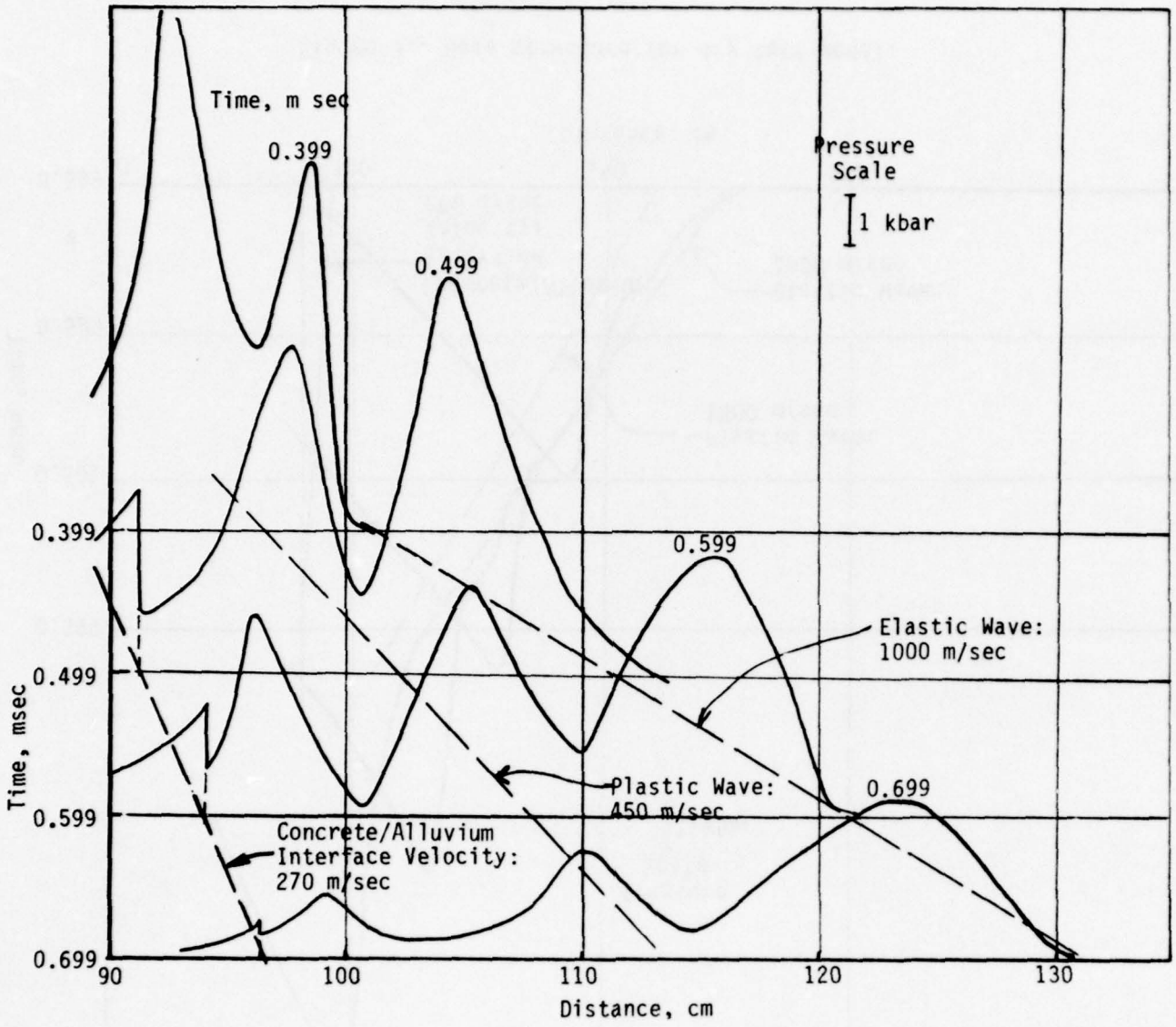

Figure 4. Wave structure for alluvium model.

It is clear from these calculations that the pressure pulses were expected to be short, approximately 0.5 to 0.7 msec, and that the distance over which the wave changes significantly is also quite short. Both effects are due to the small thickness (5 inches) of the TNT layer assumed in the calculations. The effective time interval may be on the order of 30 μsec while the effective distance may be on the order of 4 inches.

It should be noted here that both an elastic and a plastic wave are seen and that the interface - concrete/alluvium - moves with a velocity of approximately 270 m/sec.

Figure 5 shows the pressure profile as a function of distance obtained from the Sandia CHART D calculations. On the basis of these calculations, it was decided to place the pressure cells with their pressure plungers against the back face of the concrete wall. At that point, the expected pressure is 12 kbar. As will be discussed in the next section, the pressure was derated so as to accommodate lower values on the sensing samples in the pressure cells.

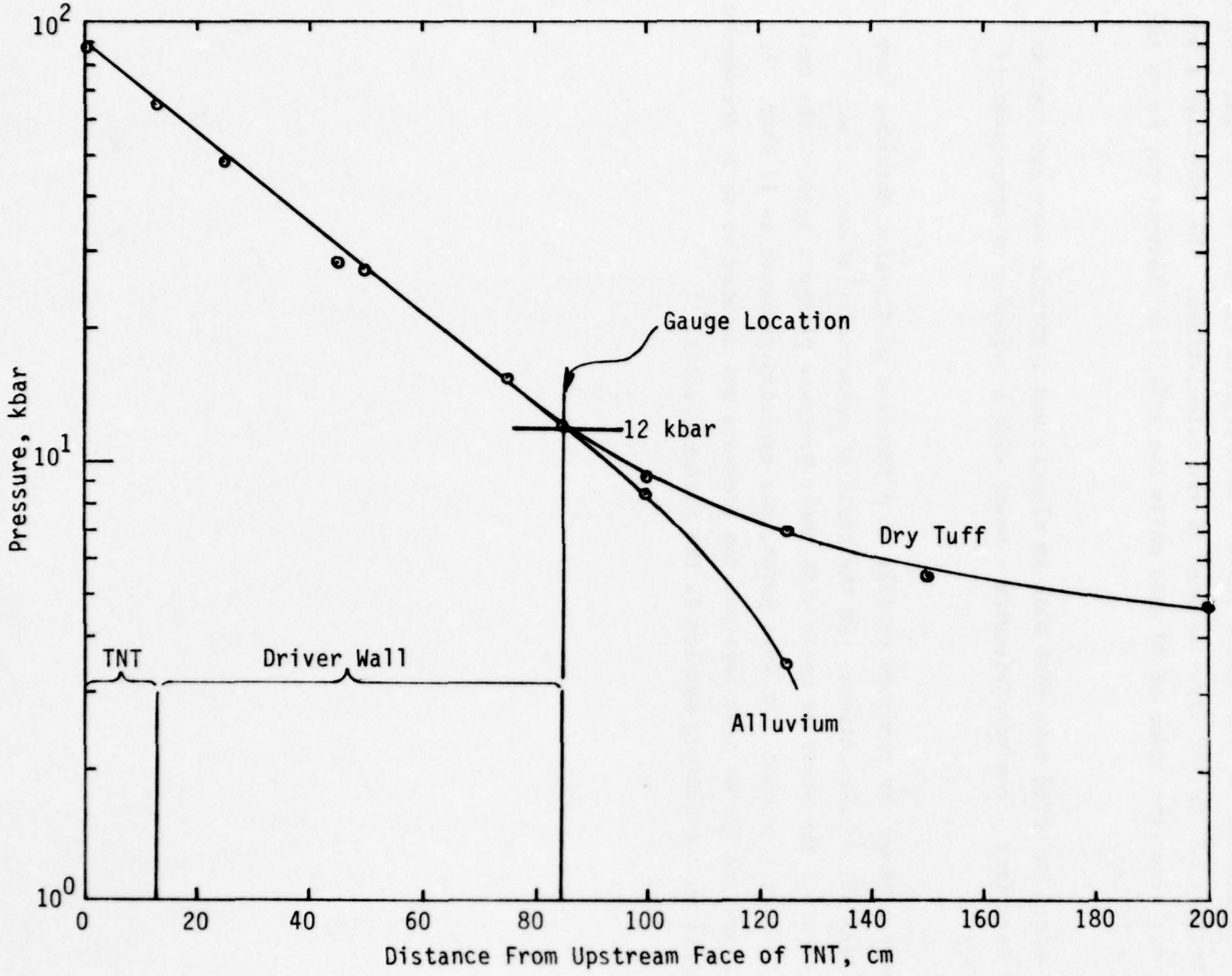

Figure 5. Pressure profiles versus distance.

SECTION IV
PRESSURE GAUGE DESCRIPTION AND DESIGN

A distinction needs to be made at this point between what is meant by pressure cell and pressure gauge. A gauge is an assembly consisting of a number of pressure cells, each cell containing a single sample that senses the pressure. In the T-5A field experiment, we assembled four metal oxide varistor (GE-MOV®) pressure cells on a steel plate to form a gauge, and three RbCl pressure cells to form the second pressure gauge.

The RbCl pressure cell operates on the principle of phase changes in the crystalline material. This phase change occurs at a pressure of about 7.5 kbar (Reference 3).* A sample of material is used as the pressure detector. It is statically loaded to some pressure P_a so that for a phase change to occur, there must be

$$P_a + P_s > P_o \tag{1}$$

where P_s and P_o are the measured shock peak pressure and the material phase change pressure, respectively. Each sample in a gauge is usually loaded statically to different values of P_a so that the shock pressure P_s will cause half the pressure cells to have their samples undergo a phase change. Since each static pressure P_a between cells differs by a constant value ε, the unknown P_s value lies between

$$P_a + \varepsilon_i < P_s < P_a + \varepsilon_{i+1} \tag{2}$$

The accuracy in the value of P_s depends upon the difference $\varepsilon_i - \varepsilon_{i+1}$ and upon the values $P_a + \varepsilon_i$ established during calibration. The value of $P_a + \varepsilon_i$ can usually be maintained within a small uncertainty, on the order of 1 to 2 percent, using strain gauges. An additional parameter controlling accuracy is the temperature changes

*This value is by no means universally agreed upon as can be seen from reading References 4 and 5. This literature gives a range between 5.4 and 7.5 kbar. At GE—TEMPO, we have observed RbCl phase changes between 6.4 and 6.8 kbar.

seen by the pressure cell because of temperature changes in the natural environment. The changes in temperature due to the shock itself are not significant, on the order of 1°C at 30 kbar in steel.

The other pressure cells use a metal oxide varistor (MOV) produced by General Electric Company (GE-MOV®). Wong and Bundy (Reference 6) have shown that MOVs exhibit pressure "memory" after being subjected to static loading. Their limit is 5 kbar uniaxially and 10 kbar hydrostatically, these limits being determined by shear and compressive strength. Their behavior under transient hydrostatic loading is currently being investigated at GE-TEMPO under separate contract.

4.1 GENERAL DESCRIPTION

Figure 6 shows a cross section of the cells used in this field experiment. It consists of two opposed flat pistons inside a pressure vessel. The cavity between these pistons and the pressure vessel contains the material sample used in sensing the pressure. It is surrounded by cast and machined AgCl to provide a near hydrostatic medium. The lower piston is screwed into the pressure cell body. When so assembled, the pressure vessel rests against a shoulder inside the body. This shoulder is only necessary until the gauge is "seasoned," meaning that it is statically loaded to a predetermined value several times prior to calibration. Once the pressure has increased once, the AgCl pill is tight against the pressure vessel wall, preventing it from slipping on the pistons. On the enlarged shoulder of the lower piston, two strain gauges (BLH SR-4) are cemented diametrically opposite one another with the wires coming out of two holes drilled axially in the piston bottom as shown in Figure 6. The upper piston has an enlarged section that rests against the lock nut. The opposite side has a pressure sensing plunger.

The pressure cell is mounted through the hole of a steel plate 3/8-inch thick with the other dimensions being 12 × 12 inches. A retaining ring and six 3/8-inch diameter bolts hold the cell in place.

A loading tube is used to apply the static load in an hydraulic press so as to avoid loading through the sensing plunger. A slot is cut in the lock nut and two flats are machined near the base of the cell body so that once loaded in the press, the pressure can be maintained by locking the nut.

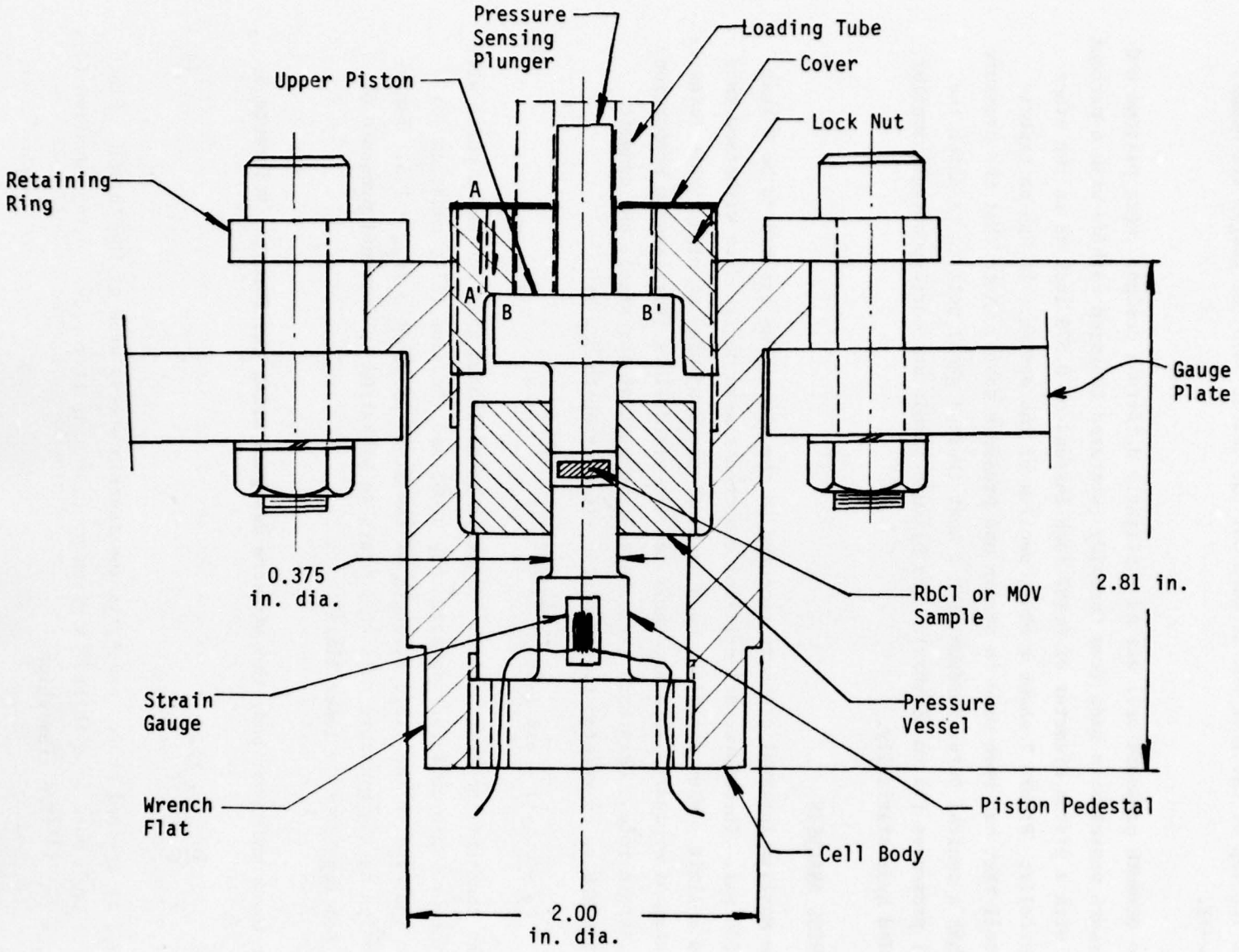

Figure 6. Cross-sectional view of RbCl and MOV pressure cells and gauge plate mounting (Not to scale).

The pressure sensing plungers face the arriving shock. A sheet metal cover is added at the top of the lock nut to keep out the cement when the gauges are bonded to the wall.

The bismuth pressure cell was of a slightly different design. Both pistons and the pressure vessel were made from Carboloy (sintered tungsten carbide with 6-percent cobalt) with a piston diameter of 0.187 inch instead of 0.375 inch as in the other pressure cells. Figure 7 shows a cross section of the design. It was an experimental cell that had been used in strain and pressure tests. Note that the pressure vessel has a conical outer surface with a heat treated steel belt to transfer the internal pressures (15 to 25 kbar). The bismuth sample was correspondingly smaller and loaded hydrostatically.

4.2 STRESS ANALYSIS

The maximum internal pressure expected on the sample was assumed to be 9 kbar or 130,500 psi. Therefore, all critical components were designed to withstand this value as a limit. When materials such as steel are subjected to high strain rates as in the case of explosive loading, their tensile yield limit increases in proportion to that strain rate. Cristescu (Reference 7) shows that for steel, the dynamic yield strength σ_y is related to the static yield strength σ_{ys} by

$$\sigma_y = \sigma_{ys} \left[1 - \exp\left(-20\tau\right)\right]^{-0.1075} \tag{3}$$

where the constants apply to steel. Since it is estimated that the shock pulse will engulf the pressure cell for approximately 0.001 sec (Section III), equation (3) gives an increase in the yield strength of the steel of about $\sigma_y/\sigma_{ys} = 1.5$. Therefore, designing the pressure cell components to withstand an internal pressure of 130,500 psi represents a lower limit.

The lower and upper body threads were designed using the formula (Reference 8)

$$\sigma_y = \frac{1}{6} \sigma_{ys} A_s^{1/2} \tag{4}$$

where σ_{ys} is defined above, and A_s is the tensile stress area of the thread. Since the force on a bolt or a thread is given by $F_e = \sigma_y A_s$ it follows, using equation (4), that $F_e = (\sigma_{ys} A^{3/2})/6$ from which

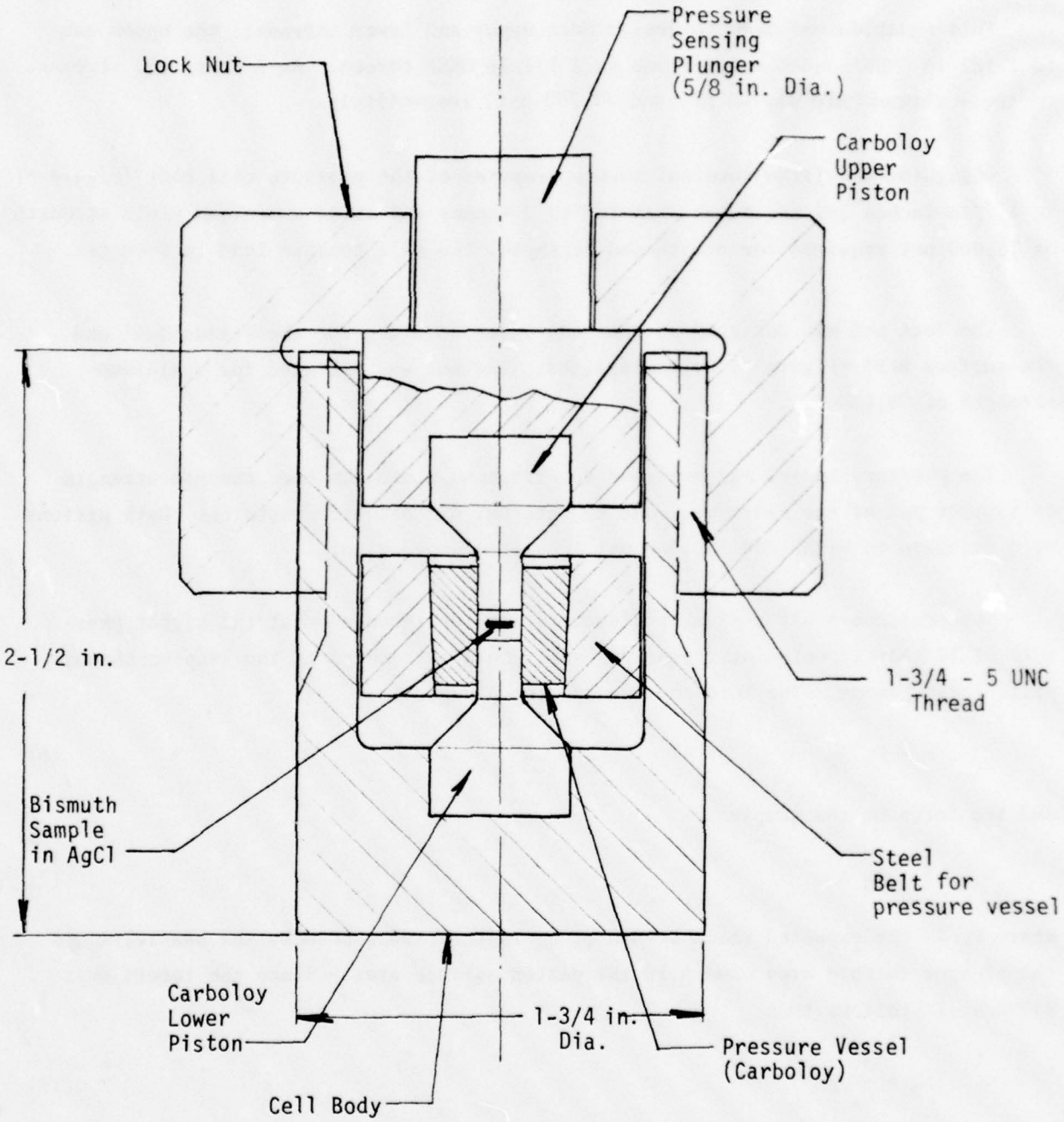

Figure 7. Bismuth element pressure cell.
(Not to scale)

$$\sigma_{ys} = \frac{6F_e}{A_s^{3/2}} \tag{5}$$

This equation was used to design both upper and lower threads: the upper one is 1 1/2-18 UNEF* and the lower one is 1 1/4-18 UNEF thread. At 9 kbar, the stresses on these threads are 41,200 psi and 72,700 psi, respectively.

Designing the large internal cavity diameter of the pressure cell body (Figure 6) to 1 7/16 inches and the outer diameter to 2 inches and using a minimum yield strength of 75,000 psi required for the thread strength, the wall tensile load is 9500 psi.

The lock nut was designed so that the stresses along the shear line A-A' and the surface B-B' (Figure 6) were minimized. The nut was designed for a minimum strength of 75,000 psi.

The pressure vessel was designed to withstand a minimum hoop tensile strength of 150,000 psi at the inner wall due to internal hydrostatic pressures. Both pistons were designed to withstand 150,000 psi in axial compression.

The pressure sensing plunger diameters were designed so that the higher pressure of 12 kbar expected at the driver wall would be reduced at the samples through piston enlargement. The force on the sensing plunger is

$$F = P_s A_p \tag{6}$$

and the force on the sample is

$$F = \sigma_s A \tag{7}$$

where P_s is the expected shock pressure, σ_s is the stress seen by the sample, A_p is the plunger surface area, and A is the piston surface area. Since the forces must balance, it follows that

$$A_p = \frac{\sigma_s}{P_s} A \tag{8}$$

*UNEF = Unified National Extra Fine—American Standard thread call out.

Table 1 shows plunger diameters to achieve stresses at the samples below 9 kbar, except for the bismuth gauge, while measuring a shock of 12 kbar.

Table 1. Sensing plunger sizes for pressure cells.

Pressure Cell		σ_s (kbar)	P_a (kbar)	P_s (kbar)	σ_s/P_s	Plunger Diameter (inches)
Bismuth		12	13.5*	12	1	0.187
MOV:	M3†	3	1	12	0.25	0.187
	M5	5	1	12	0.42	0.242
	M7.5	7.5	1	12	0.63	0.297
	M9	9	1	12	0.75	0.325
RbCl:	R4.5	4.5	3	12	0.38	0.229
	R5.5	5.5	2	12	0.46	0.254
	R6.5	6.5	1	12	0.54	0.276
	R7.5	7.5	0	12	0.63	0.297

*The phase change pressure of bismuth is 25.5 kbar at room temperature.

†Pressure cell code designation to be used throughout this report.

All parts of the pressure cells and gauge holding plates, retaining rings, etc. were manufactured by Benischek Manufacturing Co., Inc., Albuquerque, NM. Table 2 shows the list of parts, their minimum required strength, the type of steel used, and Benischek's certification of minimum yield strength in the annealed or heat treated condition.

4.3 PRESSURE SENSING ELEMENTS

The pressure sensing elements were made from RbCl and metal oxide varistors (Ge-MOV®) enclosed in AgCl as shown in Figure 8. AgCl is a waxy material that exhibits good flow characteristics at high pressures (Reference 9). The pills shown in Figure 8 are for the MOV and RbCl gauges only and consist of three parts: two end cylinders and a middle section enclosing the sample as shown. The samples were hand fitted into the middle section and then the end pieces were bonded in place using Eastman 910. This was to facilitate installation in the pressure vessel.

The bismuth pill (not shown) was essentially of the same configuration but of smaller dimensions. The bismuth sample itself had a finished metallurgical surface.

Table 2. Minimum certified strength of all pressure cell components.

Name	Steel Type	Required Design Strength (kpsi)	Annealed Tensile Yield Range (kpsi)	Rockwell "C" Hardness	Certified Tensile Yield Strength (kpsi)
Lock Nut	4340	75	80-85*	38	170
Cell Body	4340	75	80-85	--	--
Lower Piston	4340	150	80-85	38	170
Upper Piston	4340	150	80-85	38	170
Pressure Vessel	4340	150	80-85	42-43	194-201
Gauge Plate	1018†	30	35	--	--
Retaining Ring	1018	30	35	--	--
Piston Support for Bismuth Gauge	4340	150	80-85	38	170
Pressure Vessel Belt for Bismuth Gauge	4340	170	80-85	54-56	290-310

*This range of values is for hot rolled 4340 steel.

†This is hot rolled sheet steel.

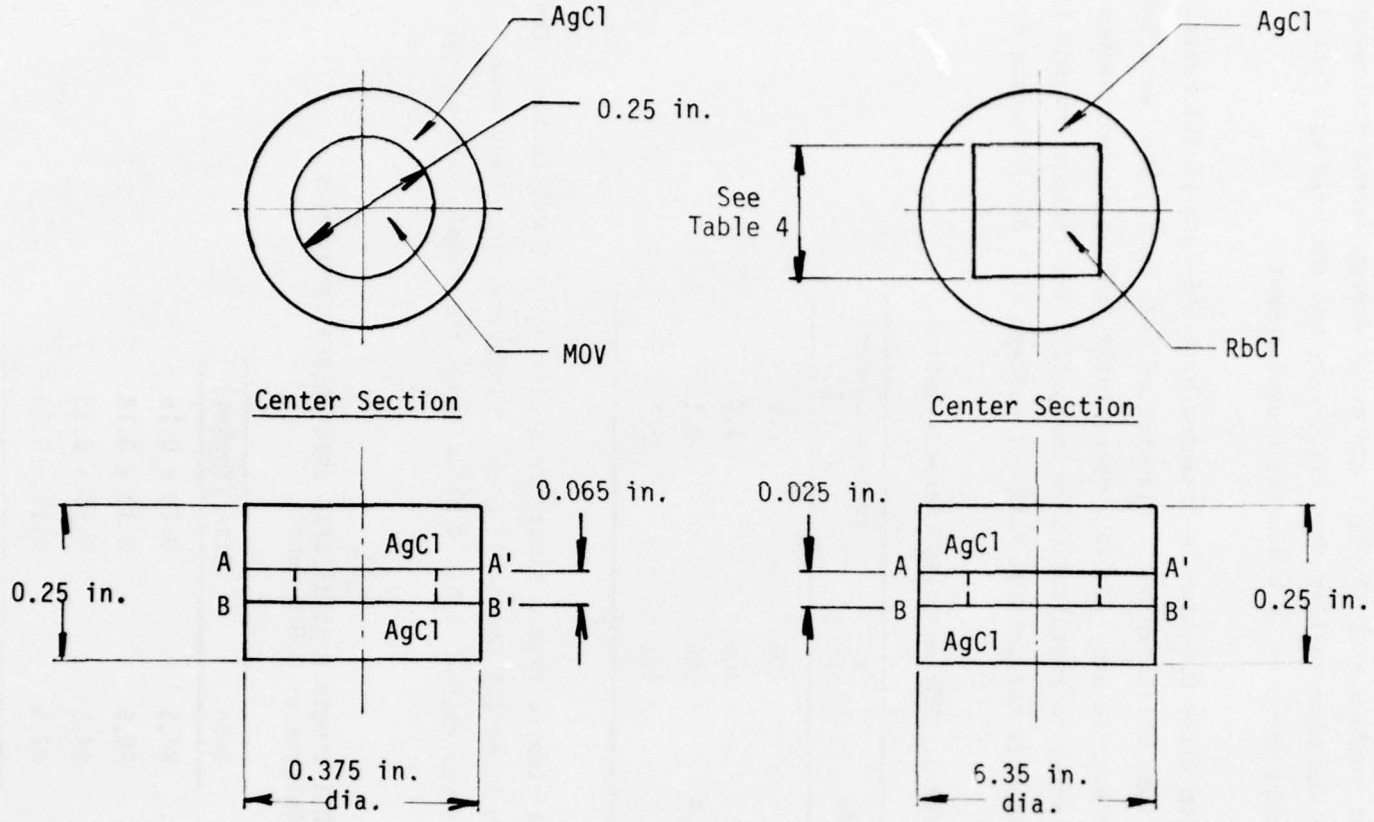

Note: Planes AA' and BB' represent separation planes. Parts as shown were bonded with small amount of Eastman 910 to facilitate installation.

Figure 8. Pressure sensing pills.

To prevent contact of that surface with the AgCl and avoid damage during preloading and shock loading, the sample was made smaller than its cavity and the void was filled with lacquer. This lacquer would serve as an hydrostatic environment.

The MOVs were cut from disks 0.8-inch in diameter by 0.065-inch in thickness. The final sample had the same thickness but a diameter of 0.25 inch. They were then annealed at 450°C for one hour in air. Table 3 shows their leakage current values at the indicated voltage prior to installation in the pill. The leakage current is defined as that current at half the initial varistor voltage at 1 mA (Reference 6).

Table 3. MOV annealed characteristics.

Code	V (volts)	Leakage Current I_L (nA)
M3	104	2.6
M5	106	3.0
M7.5	108	2.1
M9	101	2.1

The RbCl pieces were cleaved from a single crystal 1 × 1 × 0.025 inches. The crystal was obtained from Atomergic Chemicals Corp., Plainview, NY. They were simply cleaved with an Exacto knife. Table 4 below shows the sample size placed in the pills.

Table 4. RbCl single crystal size used in pressure cells (Thickness: 0.025 inch).

Code	Size (inches)
R4.5	0.20 × 0.16
R5.5	0.18 × 0.18
R6.5	0.15 × 0.15
R7.5	0.16 × 0.16

SECTION V
CALIBRATION AND FIELD INSTALLATION

5.1 CYCLE LOADING AND CALIBRATION

A set of two BLH SR-4 type FAE-12-35-S9EL strain gauges were bonded with Eastman 910 to the shoulder of each lower piston as shown in Figure 6. The strain gauge wires were run through the piston bottom holes and out of the gauge. Protective tape was placed over the strain gauges and wires and around the shoulder. The pressure cells were then assembled as shown in Figure 6 and preloaded statically twice, relaxing the force each time, before the final static loading and calibration to the values given in Table 1. This final loading was an axial force to produce an internal pressure P_a given in that table. The cycle loading was done slowly to avoid raising the temperature in the cells, thereby avoiding erroneous strain readings. The pressure cells were then mounted on the gauge plates and bolted in place with their retaining ring as shown in Figure 6. The strain gauge wires were connected to a switching box through 100 feet of wiring. This switching box was used to perform strain gauge reading after field installation and after the backfill had been put in place. Strain gauge readings were also made a few hours before firing time.

The same process was applied to the bismuth pressure cell, but upon the third loading the pressure vessel burst. The reason for this is the following: because of our tight schedule, the manufacturer had been unable to deliver the pressure vessel belt (see Figure 7). We decided to try the gauge without the belt, hoping that the Carboloy would resist the static load. When it burst, the press force had reached 5400 pounds, which corresponds to an internal cavity pressure of 13.6 kbar. We decided to keep the RbCl pressure cell number R7.5 for laboratory experiments. Therefore, only seven pressure cells were installed in the field: four MOV and three RbCl.

Table 5 gives the strain values obtained for each pressure cell for the first two loading cycles and the final calibration values.

Table 5. Cycle loading and calibration strain values.

Cell	Static Loading Force* ($\times 10^{-3}$ pounds)	Cycle Loading Strain (μinch/inch)		Calibration Loading Strain (μinch/inch)	Comments
		First	Second		
Bismuth	0	1098†	1168	1177	
	1	1189	1253	1259	
	2	1267	1330	1334	
	3	1339	1407	1410	
	4	1413	1480	1482	
	5	1528	1564	1564	
	5.4	1587	1599	--	Pressure vessel burst
M3	0	-010	-010	-010	
	1	+370	+360	+375	
	1.6	+550	+540	+550	
M5	0	801	809	809	
	1	1160	1190	1162	
	1.6	1295	1312	1355	
M7.5	0	285	290	281	
	1	584	562	562	
	1.6	670	640	640	
M9	0	-514	-515	-514	
	1	-340	-294	-288	
	1.6	-217	-193	-185	
R4.5	0	-263	-260	-260	
	1	+128	+140	+146	
	2	+377	+346	+371	
	3	+565	+511	+540	
R5.5	0	-329	-330	-330	
	1	+099	+070	+077	
	2	+389	+360	+370	
	3.2	+707	+720	+730	
R6.5	0	110	95	97	
	1	455	460	470	
	1.6	635	650	635	

*For the MOV and RbCl cells, the force can be translated into internal cavity stress by dividing the value by 0.1104 $inch^2$, which is the piston area. For bismuth, the divider is 0.0275 $inch^2$.

†Unless otherwise shown, strain values without a sign in front are positive values. Where ambiguous, signs are shown.

5.2 TEMPERATURE EFFECTS

From laboratory experiments with strain relaxation on pressure cell designs, we had become concerned about variations in the sample static loading due to changes in the pressure cell body and components due to changes in the environmental temperature. Laboratory experiments had shown that periodic fluctuations in environmental temperatures appeared as strain fluctuations. A simple analysis showed that a change of 1°C produced a change of about 10 μinch/inch in the strain readings.

Therefore, in addition to installing strain gauges on each pressure cell, we installed a single calibrated thermistor, type YSI NO.44007, with a resistance of 5 KΩ at 25°C. This allowed the monitoring of the soil temperature at the gauges over the period between installation and firing. From these temperature values, we were able to determine the changes in pre-firing static stress on the samples from temperature induced changes in strain.

5.3 STATIC LOADING VALUES UP TO SHOT TIME

Table 6 shows the values of the strain at various times between calibration in the laboratory, following field installation, and before shot time. The first column is the date and time of day for the reading. The second column gives the strain followed by the thermistor resistance with the equivalent temperature.

By the time the gauges were installed in the field, two pressure cells, M7.5 and M9, had lost some of their internal stress, later regained by an increase in the ground temperature. In the case of pressure cell R4.5, which was not pressurized, a slight pressurization did occur due to the increase in the soil temperature.

From these data, it can generally be concluded that the pressure cells held their internal pressure for 27 days without substantial changes. Any changes observed in the strain readings between the day of calibration (9/9/78) and the day of the last reading (10/6/78) can be accounted mostly by changes in temperature based on about 10 μinch/inch/°C strain change.

5.4 FIELD INSTALLATION

On September 11, 1978 both gauge plates were installed at the T-5A test site. Figure 9 shows an elevation cross section through the tunnel and driver wall, and

Table 6. Strain values and temperature of pressure cells prior to shot time.

Cell	Date and Time of Measurement	Strain (μinch/inch)	Thermistor Resistance (KΩ)*	Temperature (°C)	Comments
M3	9/9/78 8:30 p.m.	558	5.23	23.9	
	9/11/78 8:00 a.m.	527	4.80	25.9	
	10/6/78 7:30 a.m.	520	3.62	32.5	Reading jumped from 420 to 650
M5	9/9/78 8:30 p.m.	1351	5.12	24.5	
	9/11/78 8:00 a.m.	1337	4.82	25.85	
	10/6/78 7:30 a.m.	1367	3.62	32.5	
M7.5	9/9/78 8:30 p.m.	647	5.27	23.8	1) Pressure loss had occurred by 9/11/78
	9/11/78 8:00 a.m.	489	4.80	25.9	
	10/6/78 7:30 a.m.	532	3.62	32.5	2) Slight pressure gain by 10/6/78 due to rise in temperature
M9	9/9/78 8:30 p.m.	-180	5.14	24.3	1) Pressure loss had occurred by 9/11/78
	9/11/78 8:00 a.m.	-289	4.80	25.9	
	10/6/78 7:30 a.m.	-267	3.62	32.5	2) Slight pressure gain by 10/6/78 due to rise in temperature
R4.5	9/9/78 8:30 p.m.	-249	5.18	24.2	This gauge had not been statically loaded. It replaced R7.5.
	9/11/78 8:00 a.m.	-240	4.80	25.9	
	10/6/78 8:00 a.m.	-190	3.62	32.5	
R5.5	9/9/78 8:30 p.m.	755	5.11	24.5	
	9/11/78 8:00 a.m.	713	4.79	25.9	Negligible pressure loss†
	10/6/78 8:00 a.m.	735	3.62	32.5	Pressure gain due to temperature increase
R6.5	9/9/78 8:30 p.m.	658	5.18	24.2	
	9/11/78 8:00 a.m.	632	4.80	25.9	Negligible pressure loss†
	10/6/78 8:00 a.m.	678	3.62	32.5	

*A decrease in the resistance indicates an increase in temperature.

†Negligible pressure loss means a negligible loss in excess of what could be accounted for by temperature changes alone.

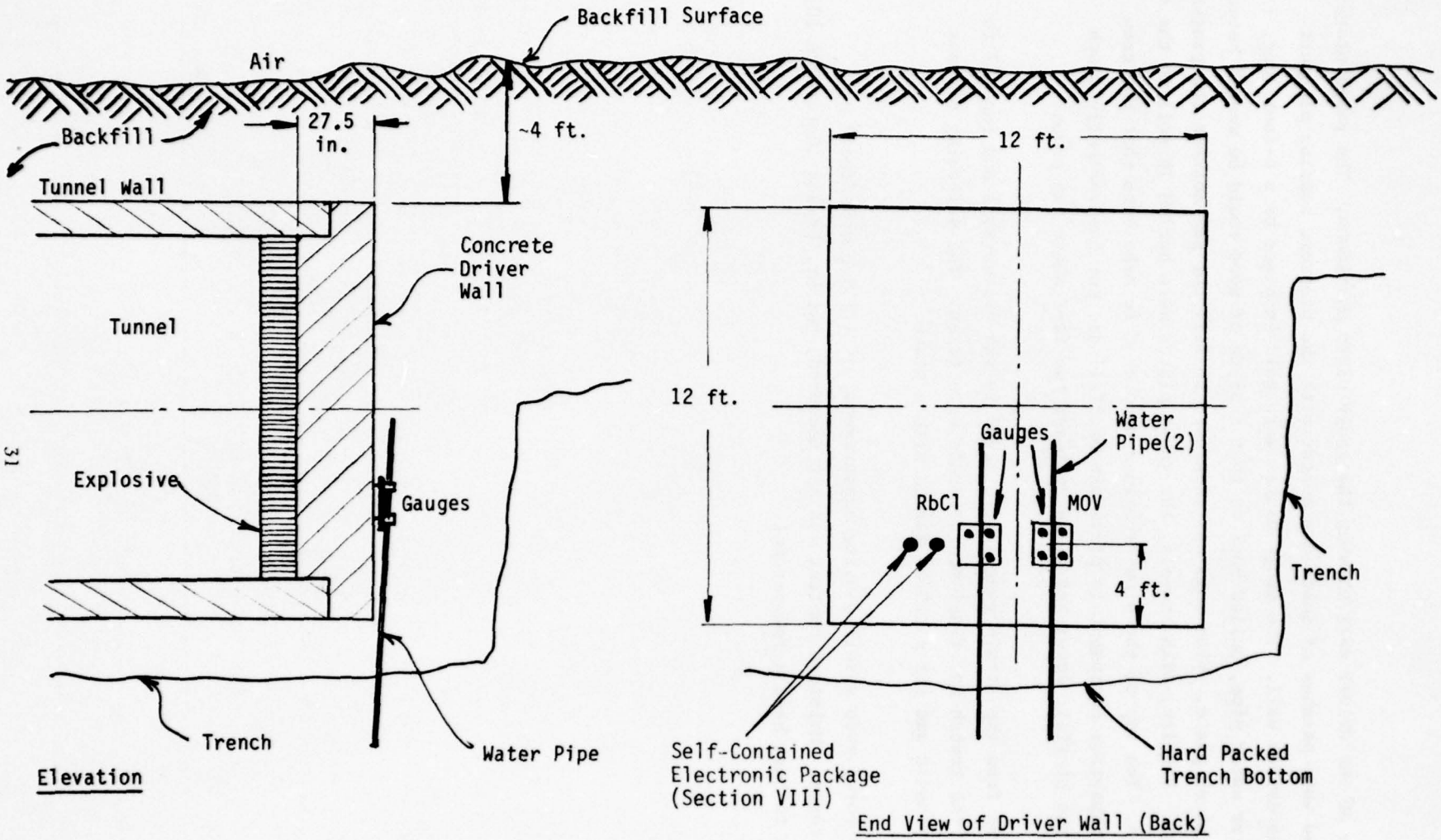

Figure 9. Gauge emplacement at driver wall.
(Not to scale)

an end view of the driver wall showing the gauge plate positions. The gauge plates were pressed into patches of quick-dry mortar with the pressure sensing plungers touching the driver wall. The gauge plates were held in place by a 6-foot long, 1/2-inch diameter water pipe, pulled back so that a piece of wood could be wedged between it and the steel plate. Fine soil was then used to fill the gap between the gauges and the wall. Finally, with shovels, the gauge plates were buried in soil to the top of the pipes. The top of the pipes remained uncovered to make sure that the crew using the compaction equipment to place the backfill did not inadvertently touch them until the backfill level had risen at least two feet above the pipes.

The wires from the strain gauges were taped to the driver wall and run off to the side of the trench and final measurements were taken. The switching box was wrapped in plastic and its position marked with a stake.

The Air Force made a soil density measurement, of 111.5 pounds/feet^3 near the gauge plates. Moisture content was not measured, but Mr. Bryant (Reference 10) believes it to have been a few percent.

SECTION VI
GAUGE RECOVERY AND POST MORTEM

6.1 SITE OBSERVATIONS AND GAUGE RECOVERY

Figure 10 shows an aerial schematic of the trench in the vicinity of the driver wall after the detonation. A crater approximately the width of the trench is shown centered about the original position of the driver wall. A large block of concrete was found some 4 to 6 feet from the original driver wall position and another large block was found some 33 feet further back on the crater lip. The original position of the driver wall is indicated by a dot marked "stake" in Figure 10. The gauge plates were found some 8 feet from their original position. One gauge plate was found in a vertical altitude but facing backward, while the second one was found lying flat facing up. They were at approximately their original position with respect to the vertical center plane, and approximately one foot above their original depth. One can containing electronic components was also recovered nearby the gauge plates (see Section VIII).

From the gauge plate positions at recovery, it can be concluded that they were driven back some 8 feet and that tumbling occurred probably over a large part of that distance. Chunks of the driver wall were found near the gauges.

The conditions of the gauge plate recovery were not expected. From the T-3 event, we had not expected the driver wall to break up into small chunks. The T-3 wall was found nearly intact (Reference 17), moved back by a small distance, and slightly inclined toward the back. We had placed our gauges in the T-5A experiment at the position indicated in Figure 9 in the hope that a similar condition as in T-3 would occur. As will be described below, we believe that this motion was responsible for the observed pressure cell deformation (see Section VII).

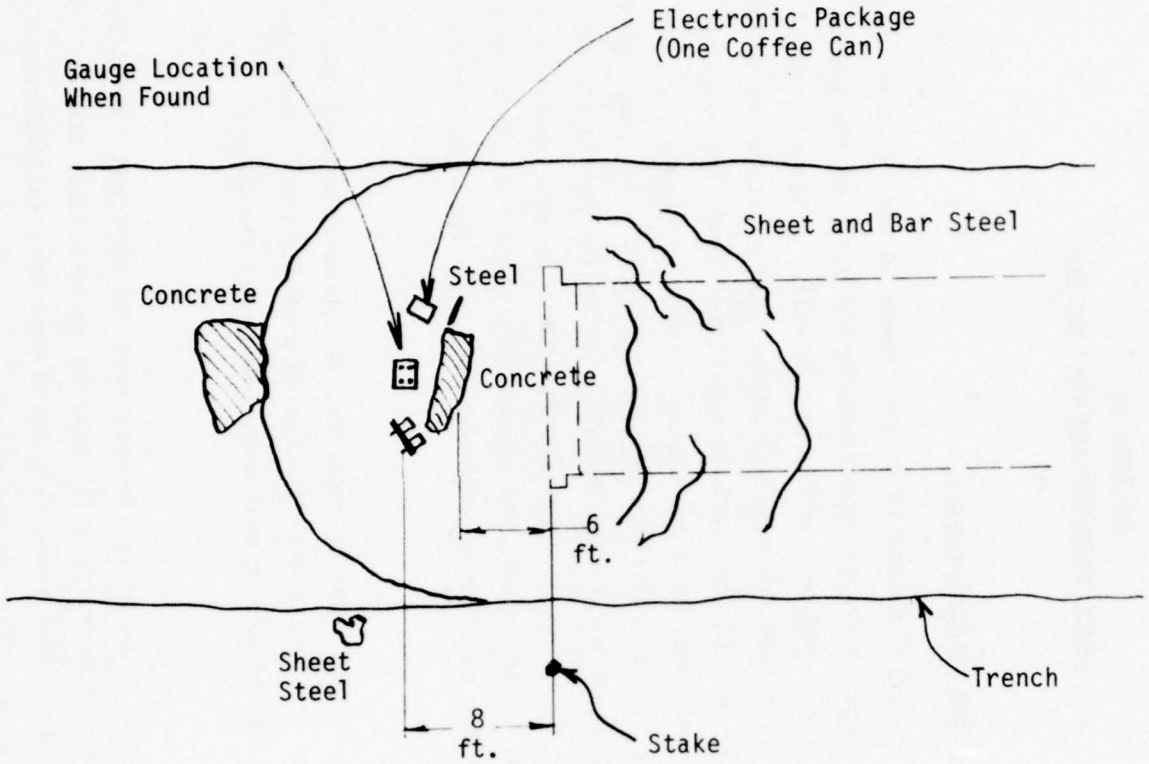

Figure 10. Post-detonation trench and crater.

6.2 GENERAL GAUGE APPEARANCE

For reference, the front and back sides of the gauges are defined in Figure 11. The dashed line indicates the alluvium compacted against the plate as a result of the explosion. The gauges were brought back from Yuma with this compacted material on them. Figure 12 shows a front and back view after most of the alluvium had been removed. Figure 13 shows the front close-up view of one of the pressure cells.

The gauges were initially packed under some 12 to 15 feet of alluvium containing lots of small milky quartz-like rocks ranging in size from microns to centimeters. The material found at the back and front face of the gauges consisted of a hard granular fine material that was densely packed and stuck to the steel and in cracks. Many small inclusions (millimeters to centimeters) were found to contain a white dense powder. This powder appears to be the pulverized and densified milky quartz-like rock referred to above.

The bulk of the soil was chiseled and hammered away until the bare metal was exposed. All metal surfaces were corroded the color of dark brown rust. It was found that the alluvium in the Yuma test area is alkaline in content which would explain the corrosion. None of the cell bodies nor the steel plates were made from stainless steel, nor had they been protected beforehand by a coating of paint or other corrosion resistance agent. This treatment was felt to be unnecessary.

First observation revealed that the gauge plate had suffered localized deformations. By and large, the plates had remained flat but locally severe deformation could be noticed, particularly near and around the pressure cell body as seen from the back face. Looking at the front, the cell body retaining rings had suffered considerable deformation; they were dished in a way as to produce an outward convexity. Considerable alluvium was trapped between the retaining ring and plate, acting as a cushion to prevent greater deformation.

Most of the retaining ring bolts were more or less severely bent and deformed. During disassembly, it turned out that 2 to 3 out of 6 bolts on the average were sheared.

All pressure sensing plungers were deformed to varying degrees. Some had suffered axial compression with lateral wall barreling, others the same effect plus

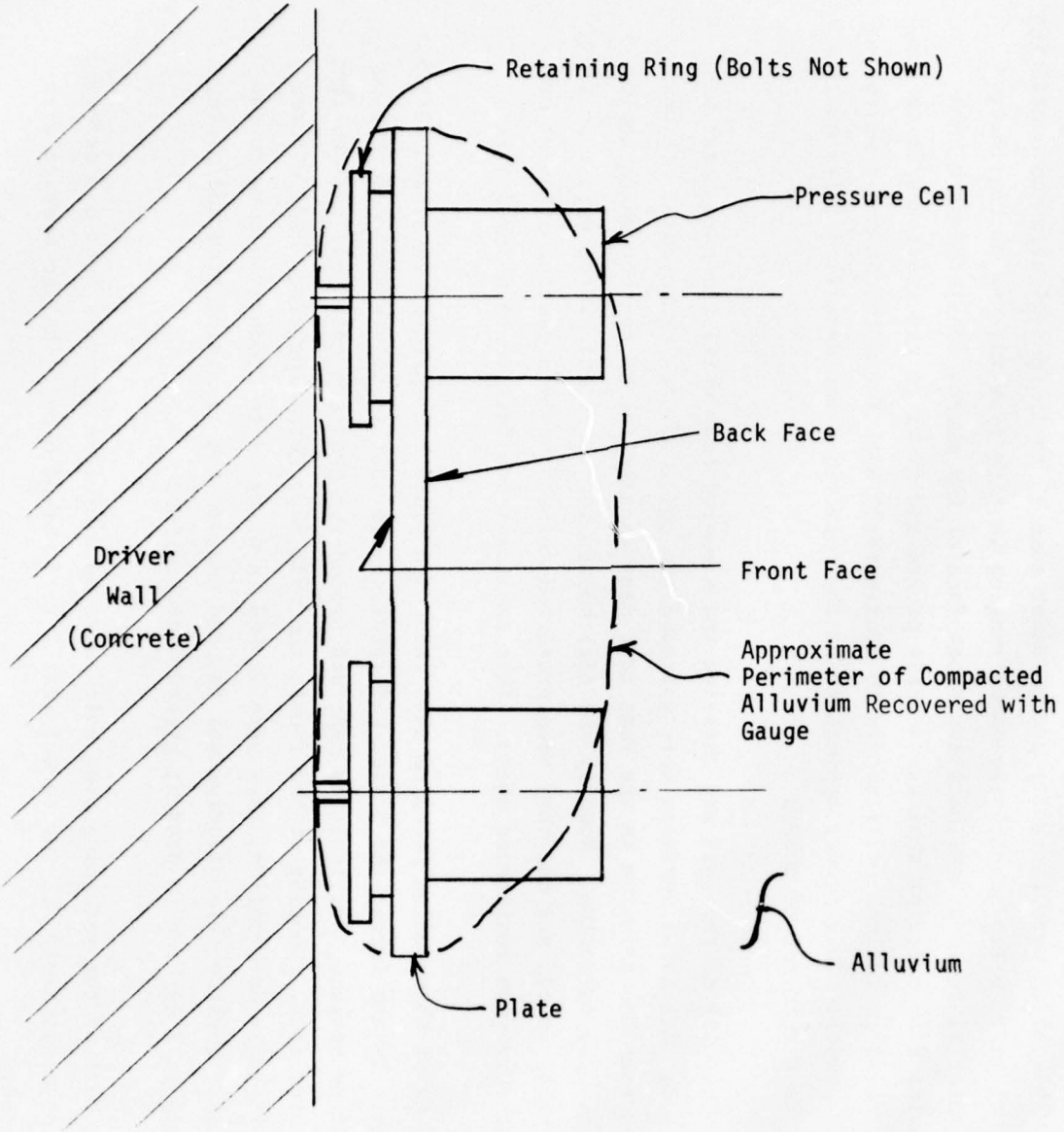

Figure 11. Gauge with compacted alluvium. (No scale)

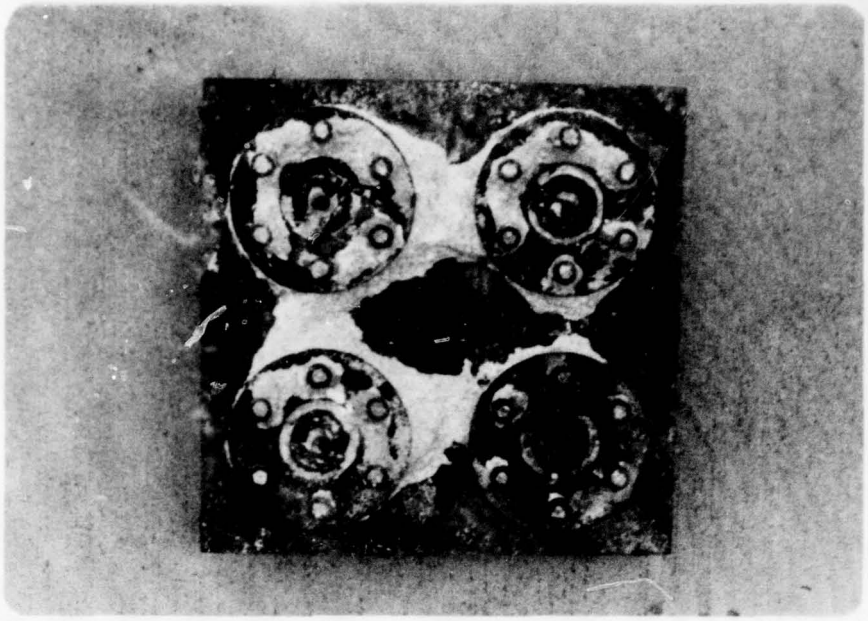

Figure 12a. Gauge (MOV) front view with most alluvium removed.

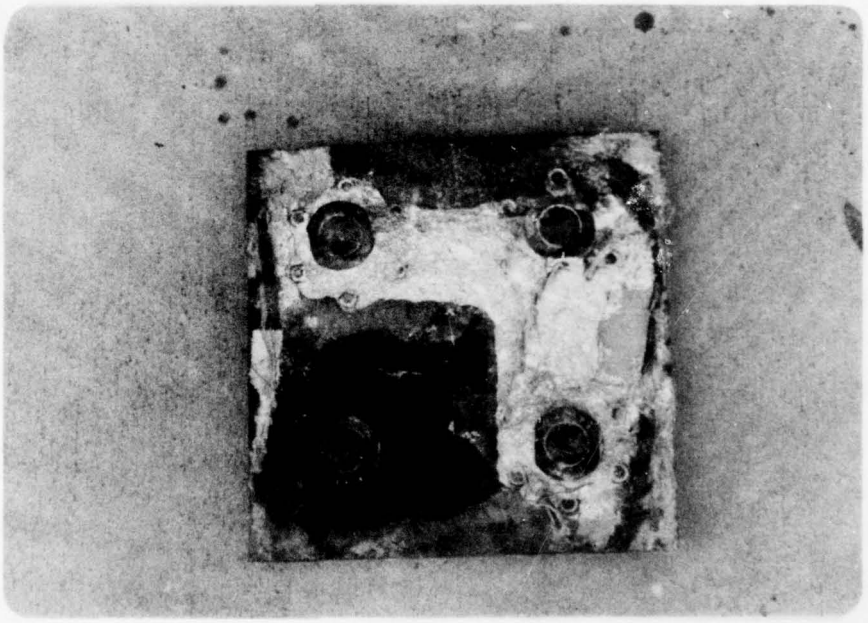

Figure 12b. Gauge (MOV) back view with most alluvium removed.

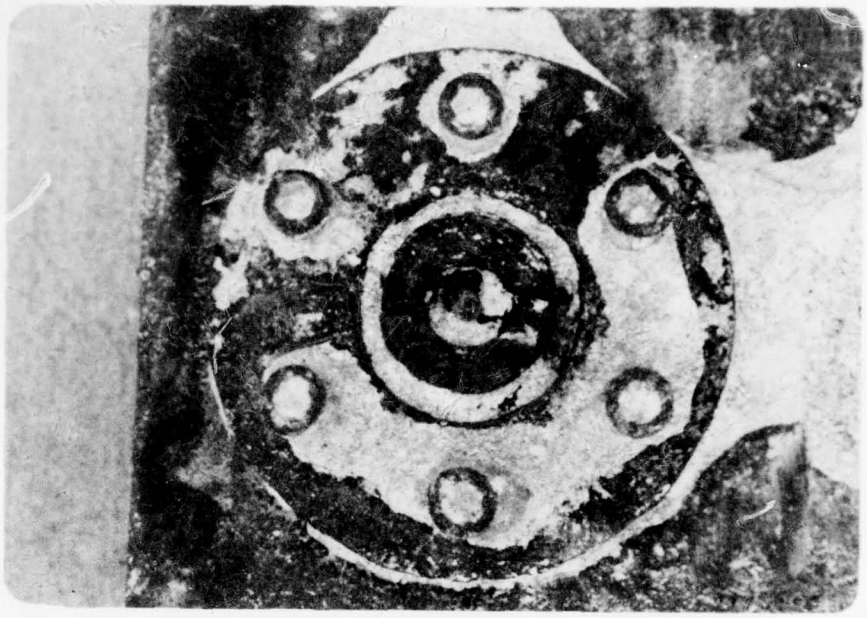

Figure 13. Close-up of front face of pressure cell.

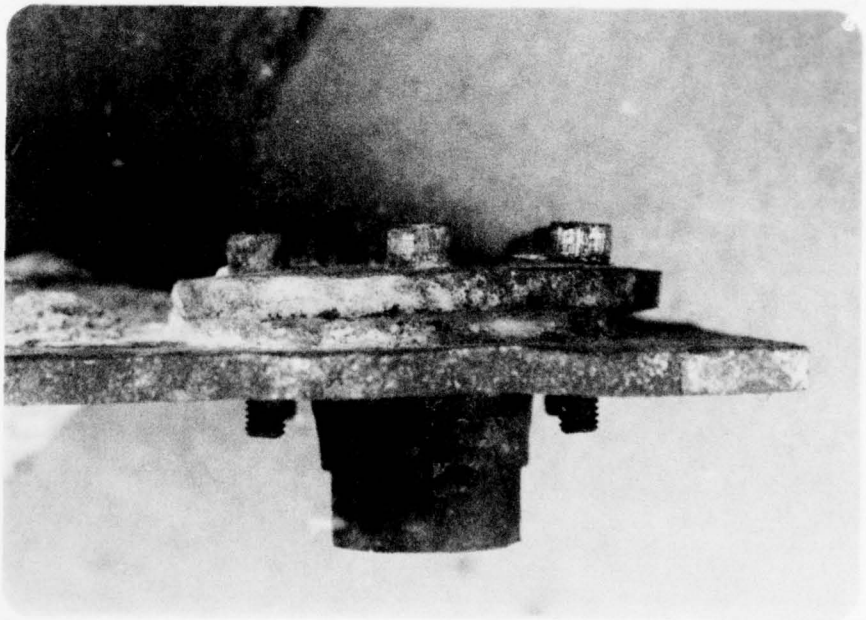

Figure 14. Side-view of pressure cell with nuts and lockwashers removed.

bending. None were so deformed that the diameter at the front edge could not be measured. Such measurements agreed with the values given in Table 1.

Looking at the rear side, the cell bodies had suffered 1/4 to 3/8-inch axial deformation due to compression. This axial shortening caused a good deal of radial barreling. It turned out that during disassembly, the barreling process had occurred along the entire cell body length and caused the holes in the plate to be enlarged, also reducing the size of the bolt holes around it. This decrease in the bolt hole size prevented them from being removed. The plate material surrounding the hole was deformed into a dish around most of the cell body periphery.

6.3 CELL BODY REMOVAL

The nuts and lockwashers holding the retaining ring and pressure cell bodies were removed. Almost all nuts were easy to loosen, indicating that most of the initial tensile load placed on them during assembly had been considerably reduced. Figure 14 shows a side view with nuts removed. The lockwashers were embedded in the steel plate by sometimes as much as 0.020 inch. After removing the nuts and the washers, the retaining rings and the bolts could not be removed even by severe hammering. Consequently, the cell body would not be removed. To remove the cell bodies from the plates, it was decided to cut through the corners with a hacksaw as shown in Figure 15. Cuts along A-A' and B-B' were made and the corner removed by hammer blow and by using a chisel inserted into the cuts. After this operation, the gauges still did not come free from the gauge plate because the cell body retaining lip was deformed and retained in place by compacted soil and large deformation of the steel. Thus, additional angular cuts were necessary as shown in Figure 16, marked by the dashed lines A-A' and B-B'. The next problem was to remove the remainder of the retaining ring. The bolts could not be turned nor hammered out through the plate. Therefore, they were sawed off between the ring and the plate using a tungsten carbide saw. These cuts were begun with bolts nearest the edge; for example, bolts C and D, shown in Figure 16. A large road pick was then inserted between the ring and the plate and the remaining bolts were snapped and the ring removed. In some cases, additional cuttings along A-A' or B-B', shown in Figure 16, were necessary before the cell body could be removed. Their removal usually still required considerable lateral hammering to free them from the plate. In one case, the retaining ring was removed without cutting into it.

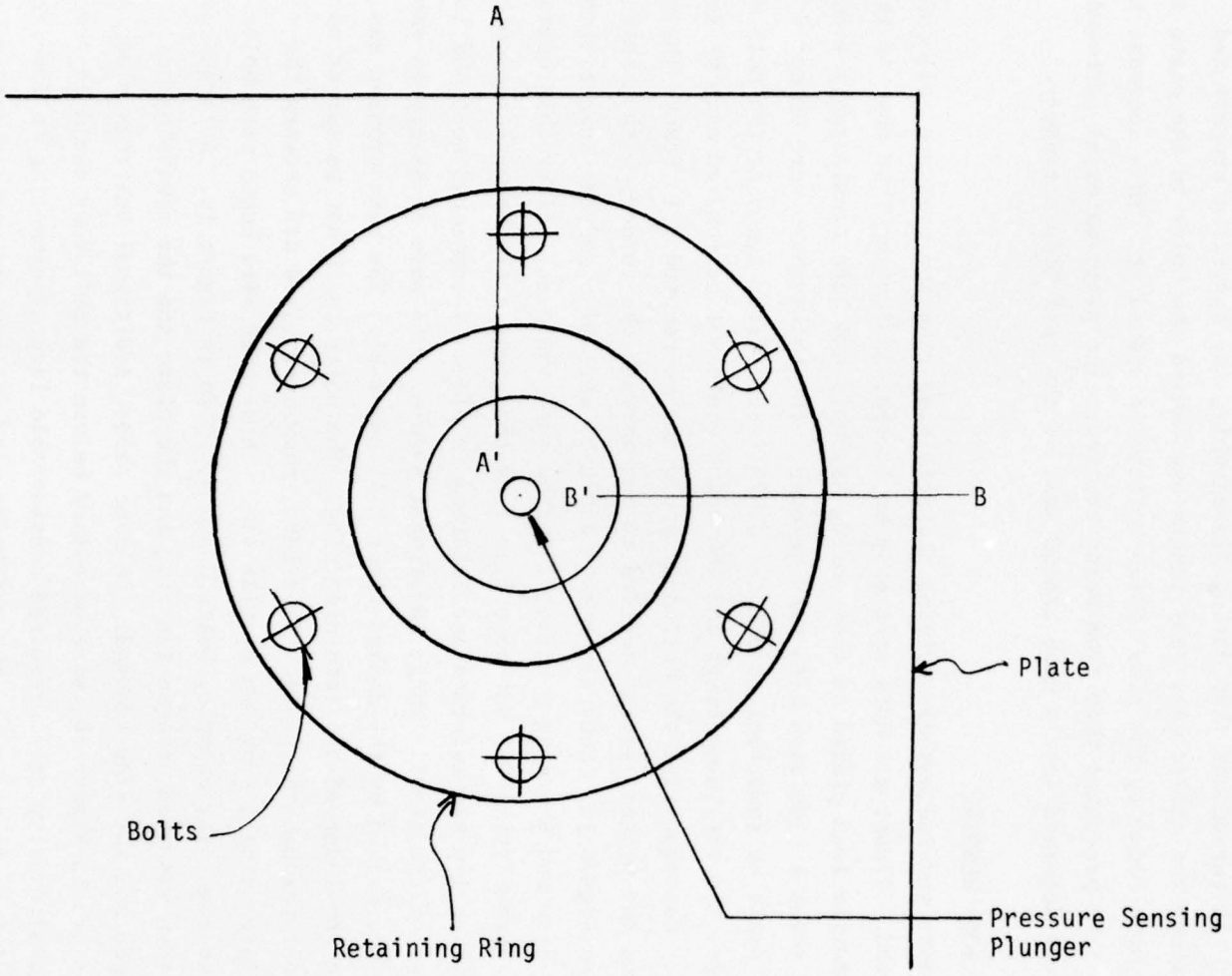

Figure 15. Saw cut positions to remove pressure cell.

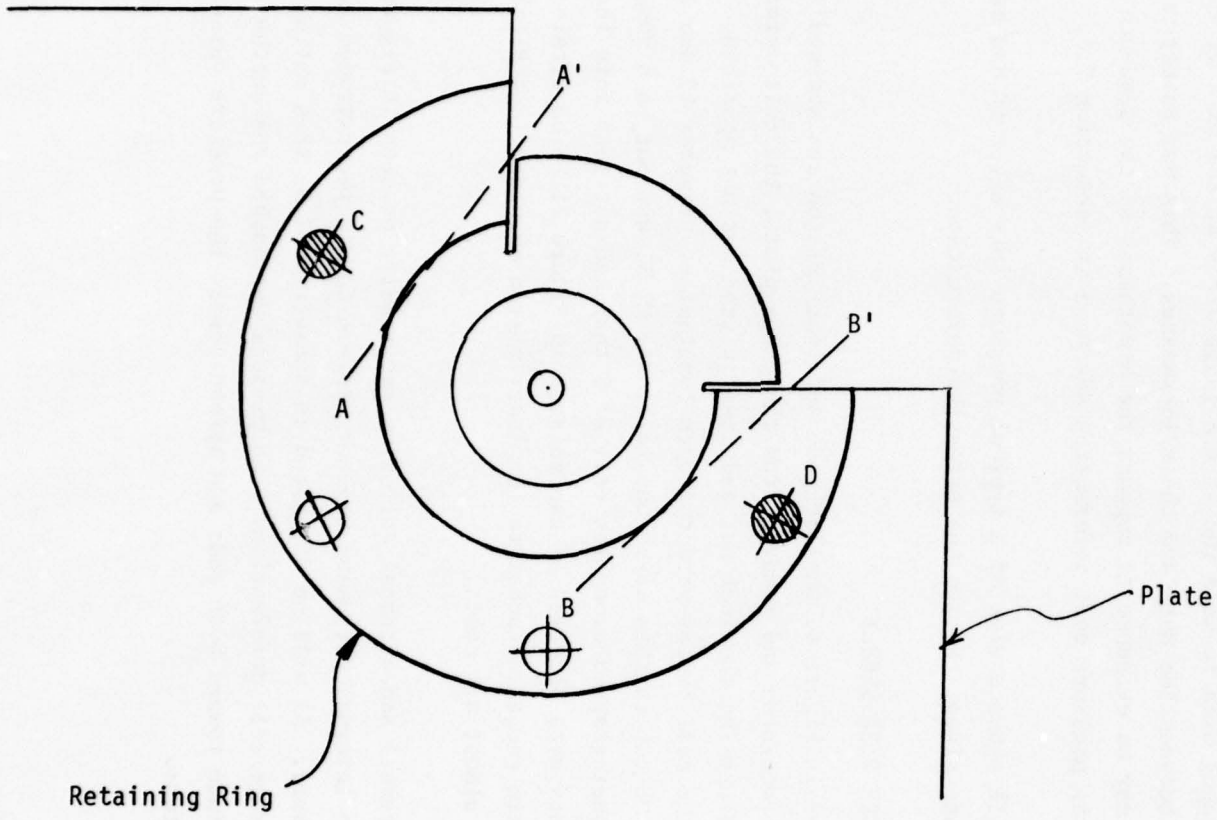

Figure 16. Additional saw cuts to remove pressure cell. Bolts C and D were also cut.

Figure 17 shows this ring. Note the extensive depression produced by the pressure cell body lip (see Figure 6). In this photograph, two bolts on the left were found sheared while the inner two were sheared during disassembly. The remaining two are a rare case where the bolt could be removed from the plate without cutting or shearing.

During removal of the nuts and lockwashes, it was noticed that some of the heavy tape (duct tape) used to hold the strain gauge wires at the back of the gauge plate was trapped between the nuts and their lockwashes. This was rather unusual. This observation may be evidence to support the hypothesis of the sequence of events leading to the pressure cell deformation advanced in subsection 7.3.

Figure 18 shows a view of a typical pressure cell after it had been removed from the gauge plate. Notice the extensive deformation.

6.4 CELL BODY DISASSEMBLY

As shown in Figure 6, the lock nut and lower piston are screwed into the cell body. When recovered and removed from the gauge plate, the cell deformation was such that unscrewing the lock nut and lower piston was not possible. Instead, using a hacksaw, the cell bodies were cut open lengthwise. Figures 19 and 20 show cell Nos. M3 and M5 cut in this way. One cell, No. M7.5, was cut in a somewhat different manner and photographed alongside cell R7.5 that had not gone into the field test. All components were deformed as can be seen in Figure 21. The strain gauge wires and the strain gauges attached to the lower piston shoulder (see Figure 6) had disappeared in almost all cases.

The internal and external corrosion can readily be seen in Figures 22 and 23. However, the internal corrosion was more severe due to the extruded AgCl from the pressure vessel. As will be discussed in subsection 7.3, this extrusion occurred during pressure cell deformation. The pistons approached one another, causing the AgCl to extrude toward both ends and spread across the pressure vessel end faces and the pistons.

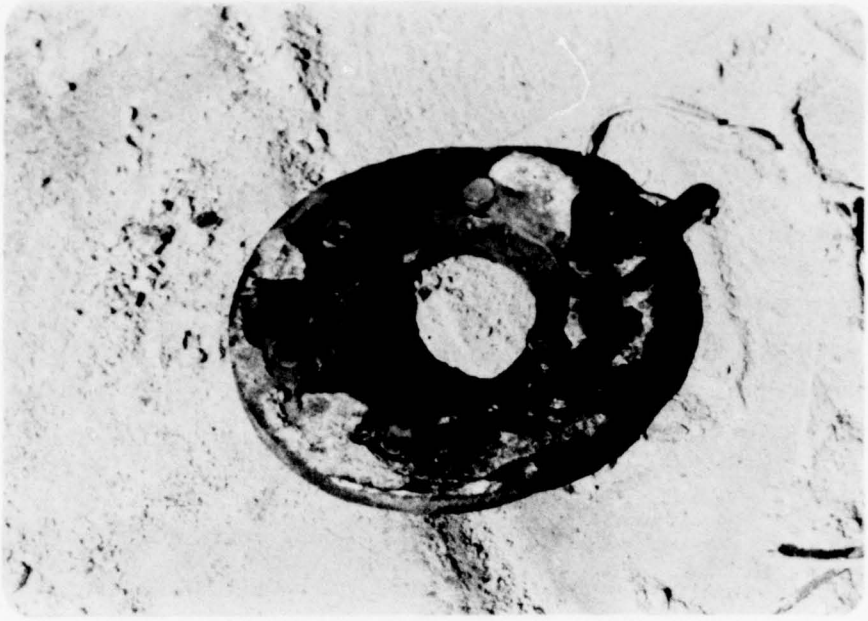

Figure 17. Typical removed retaining ring.

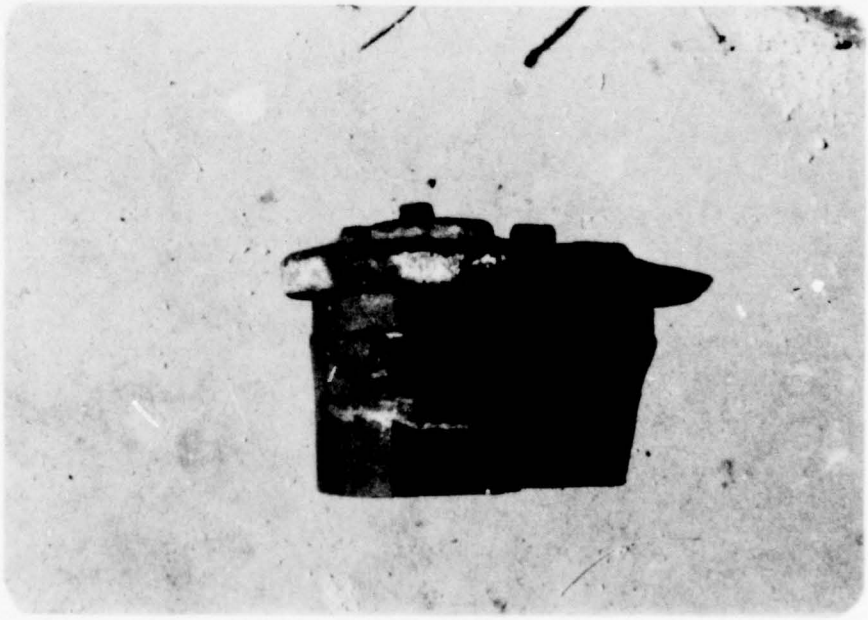

Figure 18. Typical pressure cell.

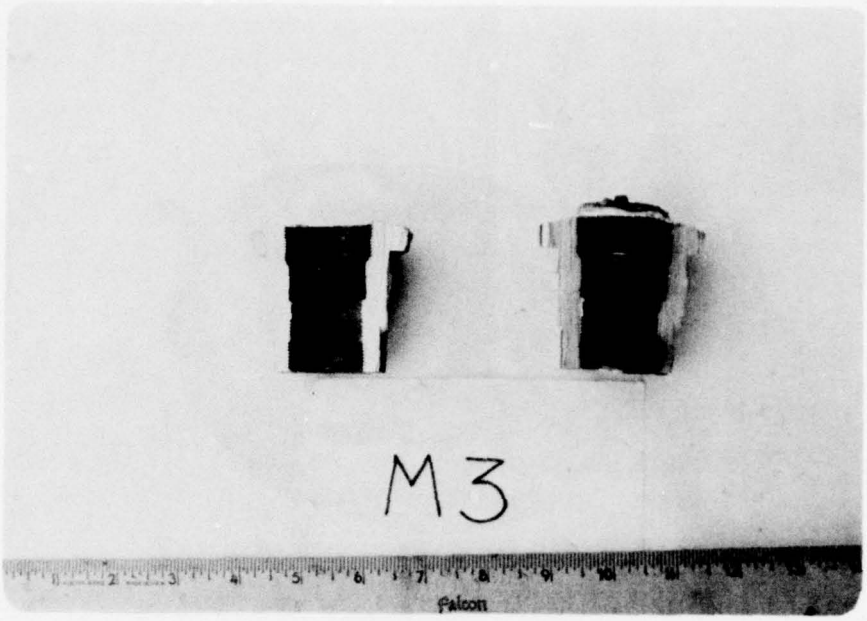

Figure 19. Sectioned M3 cell.

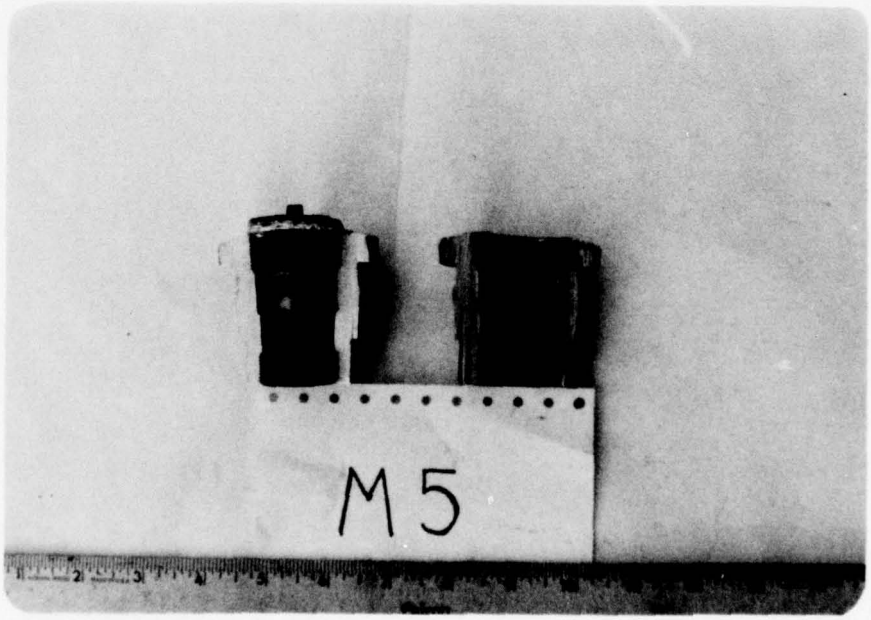

Figure 20. Sectioned M5 cell.

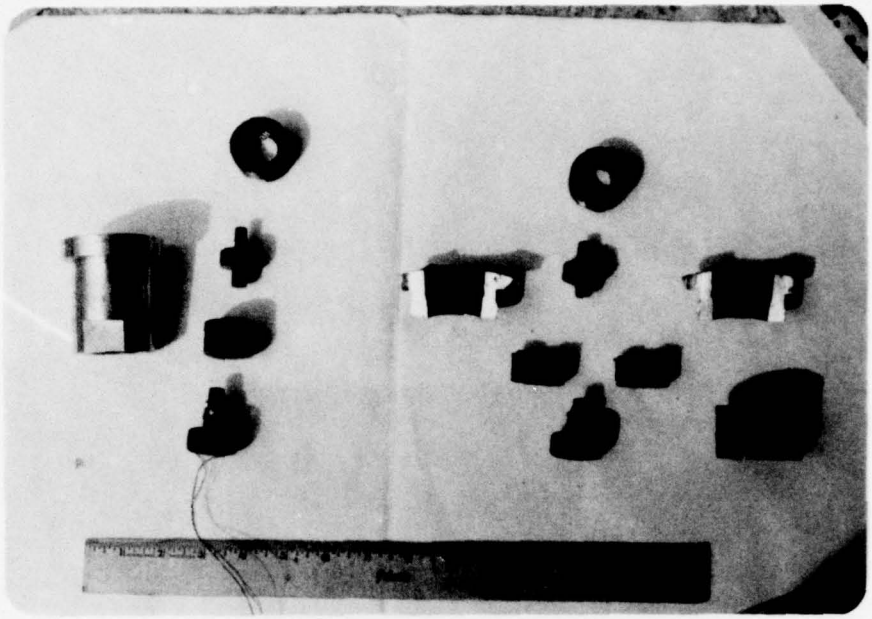

Figure 21. Comparison of undamaged and used pressure cell.

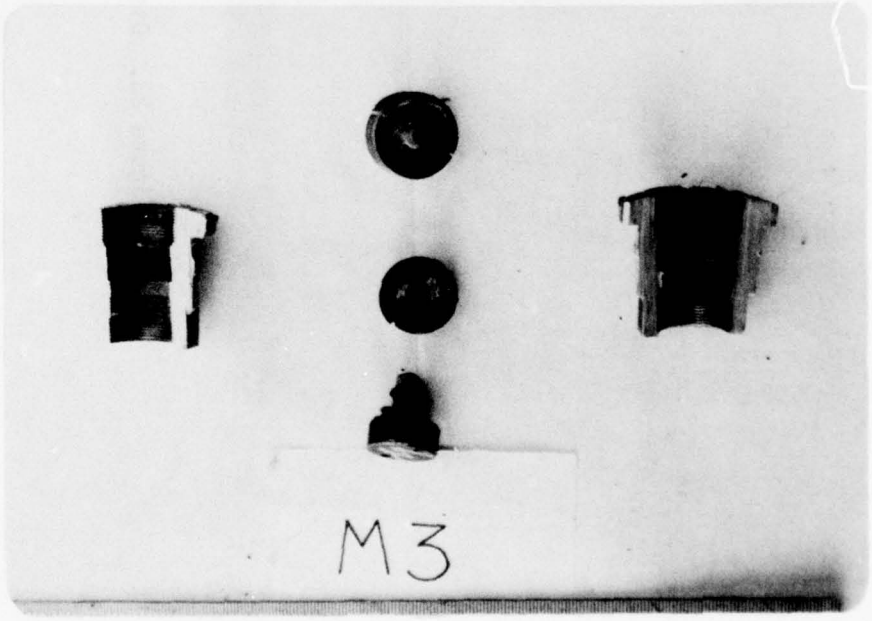

Figure 22. Disassembled M3 cell.

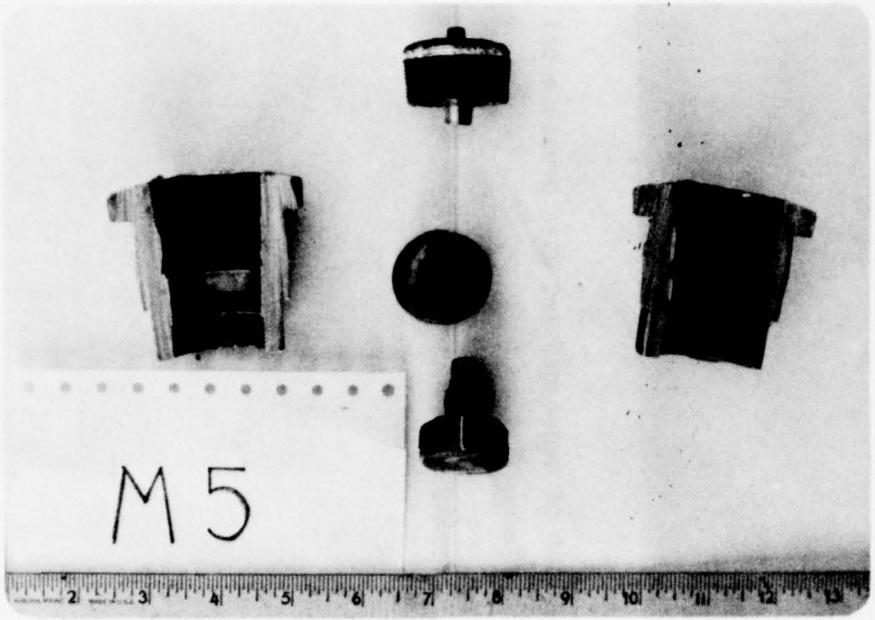

Figure 23. Disassembled M5 cell.

SECTION VII
ANALYSIS OF RESULTS

In this section, we present an analysis of the results obtained from a post-mortem appraisal of the pressure cells. Because no other pressure or displacement measurements were made in the vicinity of our gauges, no evidence exists to corroborate or contradict our findings. The analysis and the results are perforce somewhat speculative.

7.1 MOV SAMPLES

It will be recalled that four metal oxide varistor (MOV) pressure cells were installed in the T-5A field experiment. These samples were enclosed in AgCl pills whose sizes are given in Figure 8. Because of the pressure cell deformation, the MOV pills were reduced from their original 0.25-inch thickness to a range varying from near zero to 0.060 inch in thickness. In the course of disassembling the MOV pressure cells, as described in subsection 6.4, two MOVs, Nos. M7.5 and M3, were found crushed beyond usefulness.

Sample No. M5 was recovered from the remains of the AgCl pill. This pill had a final dimension of approximately 0.065 inch in thickness. The MOV sample was slightly wedge shaped with the greatest thickness of 0.063 inch and the thinnest side 0.033 inch. Its appearance was no longer circular but elliptical, with major and minor diameters of 0.300 inch and 0.255 inch, respectively. Thus, it appears as if some of the reduction in thickness went into increasing the overall diameter. From marks near the thick side of the wedge, and from its position found in the AgCl, it appears that the following process caused the deformation. As the piston faces approached one another when the cell body and other components suffered plastic deformation, they began moving out of parallelism, thereby promoting AgCl extrusion preferentially toward one side of the piston. The extrusion process entrained the sample in the direction of greatest flow and finally jammed it against the pressure vessel wall, causing the flow to deform the sample into its observed elliptical shape. The sample voltage-current characteristic was measured and it was found that

at 90 volts, the current began increasing exponentially with time from a few nanoamps to 162 nanoamps when the measurement was terminated. This runaway condition is due to the fact that during the deformation process, cracks must have developed providing paths for the current to flow in preference to the bulk material (Reference 11).

Sample MOV No. M9 was also recovered and appears to have suffered less damage than M5. The sample thickness varies between 0.058 inch and 0.061 inch compared to the original value of 0.065 inch. It is also slightly elliptical and exhibits lateral surface marks, suggesting the same process as for M5 as the cause of the deformation. However, in addition, the lower piston left a slight moon-shaped depression near the thick edge of the sample. The voltage current characteristics of M9 were measured at 90 volts. The leakage current was about 11 μA after applying the voltage for 2 minutes. The value before pressurization was 2.1 nA (see Table 3). [The duration of current measurement is usually done over a period of 1 to 2 minutes. As time increases, the leakage current also increases, but very slowly so that a 1- to 2-minute cut-off is a reasonable approach (Reference 11).] To be sure that the current was not following the external surface and the lateral surface that may have been contaminated by AgCl, the lateral side was sanded and a new measurement made. The current at 90 volts was found to be 2.5 μA and increasing, probably due to micro-cracks produced during sanding. Since the sample deformation was not too large, based on the authors' static data (Reference 18), the sample experienced a stress of about 9 kbar. This value has a large uncertainty since the estimate is based on a static data of pressure memory of a sample which had suffered deformation. However, we found in the laboratory that the current-voltage characteristic was not particularly sample shape-dependent. Thus, a possible lower limit to the shock pressure is 9 kbar, with very low confidence.

7.2 RbCl SAMPLES

It will be recalled that only three RbCl pressure cells were placed in the T5-A field test. Of these, all three samples were recovered.

Sample No. R4.5 was recovered from the AgCl pill whose final thickness was about 0.035 inch and the sample thickness was about 0.003 inch. The sample

appearance is one of extensive flow. It had spread from its initial dimension of 0.20 × 0.16 rectangle (see Table 4) across the entire pill diameter. Although the crystal suffered extensive shear during this flow process, rendering it slightly translucent in appearance, no phase change could be detected. (A phase change in RbCl crystal changes its appearance from the transparency of glass to a white milky opaque solid.)

Sample No. R5.5 underwent basically the same process as for R4.5 with a final thickness of about 0.003 inch and the crystal spread over the entire pill area due to flow. The slight translucent appearance indicates that no phase change occurred.

Sample No. R6.5 was recovered nearly in its original shape. Its size had changed from 0.15 x 0.15 x 0.025 inch to a thickness of about 0.020 inch and other dimensions approximately 0.23 x 0.23. It was not possible to estimate a volume change from its original to its final volume. [Phase change in RbCl is accompanied by a 14-percent change in volume (Reference 4), something that could not be ascertained here.] This sample showed no visual evidence of having undergone a phase change.

Using the strain gauge readings prior to the detonation, it was possible to determine the actual static loading. Using these data and the ratios of piston-to-pressure sensing plunger areas, some upper limits were placed on the stress sensed by the RbCl. These values are given in Table 7.

Table 7. Upper limit of shock pressure estimated from RbCl appearance.

Cell Number	Total static stress before detonation (kbar)	Shock pressure (kbar) for a phase change
R4.5	4.61	12.3
R5.5	7.50	16.4
R6.5	7.60	14.0

The static stresses increased because of increases in alluvium temperature over the temperature at which the cells were calibrated. Since the sensing element experienced the shock before the extensive deformation effects of the cell, any

phase change in the material would very probably have remained even though the RbCl had subsequently experienced considerable flow. Consequently, it is believed that the shock pressure at the back of the driver wall did not exceed 12.3 kbar. (The value estimated with CHART D was 12 kbar.) This fact is at least in agreement with Renick's statement that the explosive yield on T-5A driver was less than had been expected (Reference 12).

7.3 ANALYSIS OF CELL DEFORMATION

Figure 24 shows a composite cross section of the pressure cell body after sectioning. It represents a composite from all seven cells placed in T-5A. Table 8 shows some of the component dimensions indicated by letters on Figure 24. The average values of the deformations are given below each column and are to be compared with the original cell dimensions. The strain is given at the bottom of every column and defined in Reference 13 as

$$\varepsilon = \int_{\ell_o}^{\ell} \frac{d\ell}{\ell} = \left| \ell n \left(\frac{\ell}{\ell_o} \right) \right| \tag{9}$$

where ℓ_o is the initial dimension and ℓ is the final dimension. Table 9 gives the critical strain comparison between the strain for the sum of the values of columns D and F and compares these values with the strain on the body. The percentage difference between these sets of values is given in the last column.

It can be noted that the strains for the sum of piston dimensions match the axial cell body strains fairly well except in the cases noted to have badly distorted lower pistons. The distortion in these cases was mostly radial barreling to accommodate flow.

We will now describe what we believe to be the sequence of events that caused the observed deformations. Figure 24 shows a composite of deformation for all cells. An important distinction must be made between the deformations at the front of the gauge plate and the deformation at the back. The deformation at the back and the general appearance of the internal components gives the clue as to the sequence of events to be described. First, we describe the pressure cell appearance.

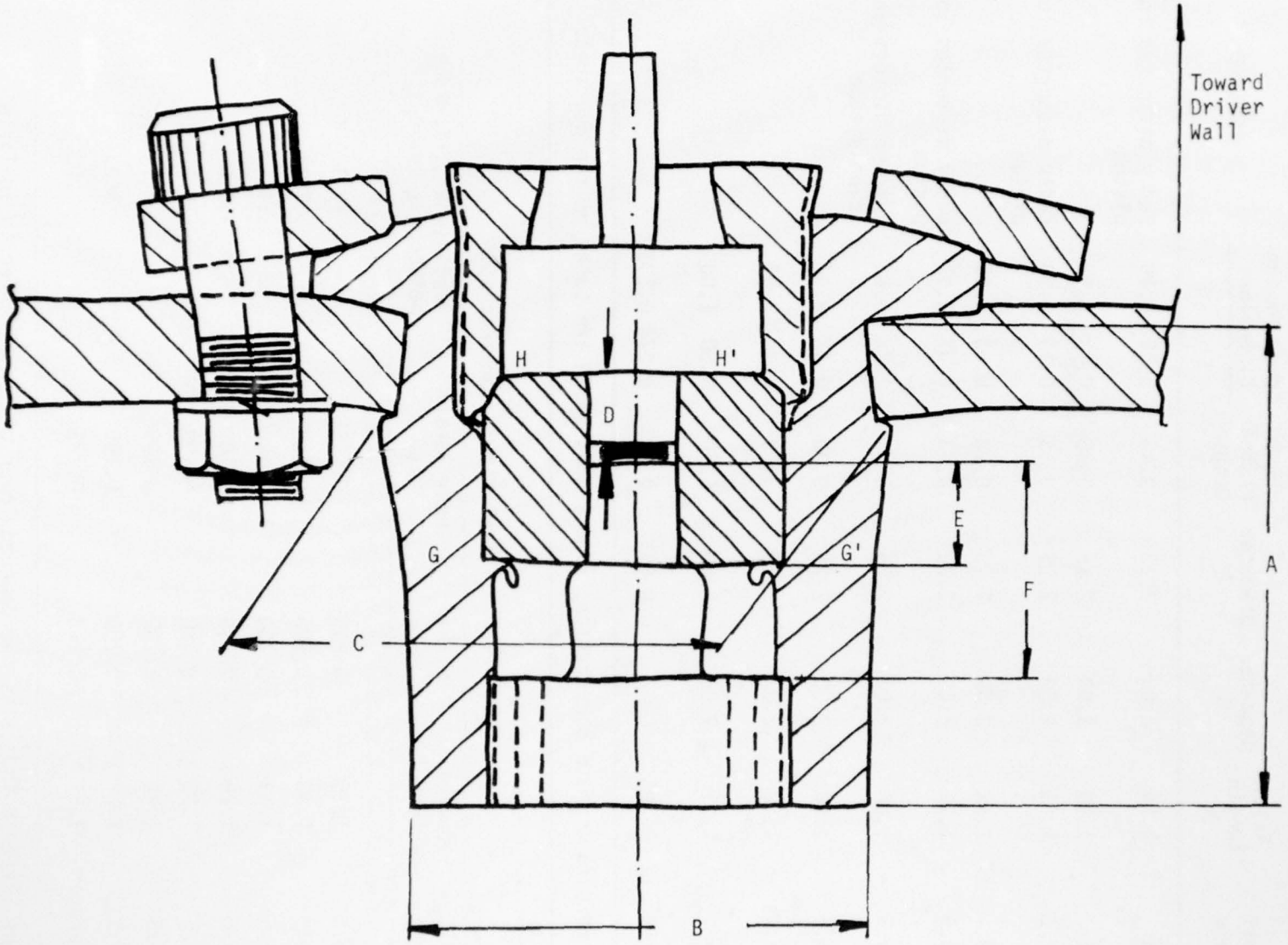

Figure 24. Composite of pressure cells after test (free-hand drawing).

Table 8. Dimensions of pressure cell elements used in deformation analysis (see Figure 24) (all dimensions in inches).

Cell Name	Axial Length A	Diameter B	Diameter C	Upper Piston Length D	Lower Piston Dimensions E	Lower Piston Dimensions F	Comments
M3	1.94	2.00	2.13	0.45	0.35	0.90	Badly distorted lower piston
M5	1.93	2.00	2.15	0.35	0.43	0.98	
M7.5	1.93	2.00	2.15	0.43	0.34	0.90	Badly distorted lower piston
M9	1.92	2.00	2.20	0.28	0.43	1.00	
R4.5	1.91	2.00	2.22	0.43	0.37	0.90	Badly distorted lower piston
R5.5	1.90	2.00	2.25	0.47	0.28	0.83	Extreme distortion of lower piston
R6.5	1.90	2.00	2.25	0.30	0.43	0.97	
Averages	1.92	2.00	2.19	0.39	0.38	0.93	
Original Dimensions	2.31	2.00	2.00	0.50	0.50	1.06	
Strain*	0.185	0	0.091	0.248	0.274	0.131	

*See text for strain computation. The values shown are based on the averages.

Table 9. Critical strain comparisons.

Cell Name	Sum of D and F	Strain ε_{D+F}	Body Strain ε_A	Percentage Difference between ε_A and ε_{D+F}*	
M3	1.35	0.145	0.175	17.1	D
M5	1.33	0.160	0.180	11.1	
M7.5	1.33	0.160	0.180	11.1	D
M9	1.28	0.193	0.185	- 6.6	
R4.5	1.33	0.160	0.190	15.8	D
R5.5	1.30	0.182	0.195	6.7	D
R6.5	1.27	0.206	0.195	- 5.3	
Averages	1.31	0.173	0.185	7.0	

*The letter D indicates the damaged lower piston referred to in Table 8.

The retaining ring was found to be deformed to produce a convexity outward with the bolts bent outward. The cell body flange had been severely squeezed and thinned out as shown. The lock nut was also deformed but only that portion that remained outside the cell body. The steel plate near the body was generally deformed with a curvature as shown. This curvature was only along a portion of the plate around the body. These deformations can be seen in Figures 14, 17, and 18.

From the back, the deformation was mostly axial, again as seen from Figures 14 and 18. The upper pistons were found shortened by amounts given in Table 9, with the large diameter section that stops against the lock nut to have been "extruded" to fill the lock nut volume. No shear marks were found on the lock nut threads. The lower piston had moved toward the front with the threads suffering no shear. However, the piston and shoulder were found more or less severely deformed. The pressure vessel was moved toward the front by the stop surface G-G' (see Figure 24) in the cell body. When the pressure vessel stopped against the lock nut, the pressure vessel produced the curled lip at the stopping plane G-G'. The body in collapsing expanded radially inward and outward. The inward expansion stopped against the pressure vessel while the outward expansion continued against the steel plate, enlarging the hole and also bulging out past it as indicated by diameter C in Figure 24. The upper surface of the pressure vessel stopped aginst the upper piston surface H-H' (see Figure 24) with the corner engaging the lock nut and producing an angle bevel. In terms of the sequence just described, it is significant to note here that:

- The threads remained intact (except for those that were unengaged in the body), and
- All component displacements occurred from the back.

The shock arrived through the driver wall and passed the pressure cell engulfing it at one time, thus loading it nearly hydrostatically. From CHART D calculations given in Section III, this hydrostatic pressure lasted approximately 0.001 second with a peak pressure less than 12 kbar. Using equation (3), we find that the static yield stress increased to

$$\sigma_y = \sigma_{ys} \left[1 - e^{-20(0.001)}\right]^{-0.1075}$$
$$= 1.52\ \sigma_{ys}$$

Since the pressure cell body was certified to have a minimum yield strength of 85,000 psi, the dynamic yield of the cell became

$$\sigma_y = 1.52(85{,}000) \simeq 130{,}000 \text{ psi}$$

or about 9 kbar. Since the internal components had higher static yield strengths (pistons: 170,000 psi), it is safe to assume that on the whole the total cell must have exhibited a dynamic yield strength greater than this, at the most a value $\sigma_y = 1.52(170{,}000) \simeq 260{,}000$ psi or 18 kbar. It is more likely to have been around the shock pressure. Therefore, it would appear that the hydrostatic pressure produced by the engulfing shock, which lasted a very short time, could not likely produce the observed deformations because of the inertia of the material. What is against the hypothesis of hydrostatic deformation is the general appearance of the deformed components; i.e., deformed as if produced by a blow from the back, which would not have been the case from hydrostatic loading. Unlike in blasts in air, the refracted wave must have been much weaker than the incident one so that this argument also cannot be invoked as an explanation.

What most likely happened is the following. After the shock passed and registered on the samples, the concrete driver wall and alluvium packed between it and the gauge plate pushed the plate and cell back against the alluvium in back of the plate. The driver wall disintegrated and the mass velocity produced the deformation seen at the front. This was followed by the plate being set in motion relative to the alluvium and then driven into the alluvium some distance. The initial velocity was very high, decaying rapidly over a relatively short distance. This motion caused the cell body to collapse axially, pushing the lower piston into the pressure vessel displacing the sample pill toward a new position further forward. When the pressure vessel stopped against the lock nut, the lower piston continued to move and AgCl extrusion began. Also, the upper piston began to "extrude" into the volume of the lock nut. Finally, the cell body continued its motion until inward and outward radial expansion stopped against the pressure vessel lateral wall and the hole in the plate. This total deformation process occurred very rapidly, while the velocity was still quite high, and consequently over a short distance. The remaining distance covered by the gauges to their resting place produced no further plastic deformation. Tumbling thus began early in the motion and probably while the crater scouring process was going on.

An attempt was made to quantify this description, and what follows is somewhat speculative. However, the results appear to be intuitively correct. From Figure 4, the concrete/alluvium interface velocity after the shock has passed is approximately 270 m/sec. In the absence of particle velocity measurements,* we can assume this value for our analysis. We assume a velocity-distance relation

$$v(x) = cx^m \tag{10}$$

By using the end points as the back face of the driver wall and the resting place of the gauge plates, the constants cannot be found. By shifting the coordinate axis toward the front face of the concrete and requiring the velocity at the resting place to be about 1 m/sec, equation (10) becomes

$$v(x) = 48.4(x + 0.61)^{-3.48} \tag{11}$$

Table 10 shows v in m/sec as a function of the distance away from the back face of the driver wall. This table shows that the velocity does indeed drop rapidly with distance.

Table 10. Velocity versus distance from equation (11).

x (m)	v (m/sec)
0	270
0.25	81.2
0.50	33.7
1.00	9.2
2.00	1.7
2.44	1.0

Integrating equation (11) gives the time-distance relation

$$\tau = 0.0046(x + 0.61)^{4.48} \tag{12}$$

At $x = 0$, $\tau \underset{\sim}{\sim} 0.0005$ second, which is small compared to the values of τ at which it is believed the plastic deformation stopped.

*Measurements made by CERF on T-3 indicate that the concrete surface velocity was 230 m/sec (Reference 14).

If the assumption is made that by the time the plate velocity had dropped by 80 percent, the deformation essentially stopped, then we can find the distance and the time from equations (11) and (12). Solving (11) for x and setting $v_f = 0.2\ v_o$ where $v_o = 270$ m/sec, there results

$$x = \left\{\frac{48.4}{0.2(270)}\right\}^{0.287} - 0.61 \tag{13}$$

$$= 0.36 \text{ m}$$

Using this value in equation (12) gives

$$\tau = 0.0046(0.36 + 0.61)^{4.48} \tag{14}$$

$$= 0.004 \text{ sec}$$

From this, it appears reasonable that most of the velocity decayed within 36 cm from its initial position and in approximately 4 msec.

We will now attempt to estimate the stresses that caused the observed cell body deformation. No elastic/plastic stress-strain data for 4340 steel could be located. Instead we used a stress-strain curve from Reference 15, shown here as Figure 25, for 1045 steel. From Table 8, the cell body strain based on the average of all measurements is 0.185 so that from Figure 25, the stress is approximately 140,000 psi or 9.7 kbar. On the basis of the deformation of the upper piston where the average strain is 0.248 (Table 8), Figure 25 gives a stress of about 145,000 psi or 10 kbar. From such an analysis, it appears that the force developed by the motion of the gauge plate in the alluvium resulted in stresses on the order of 10 kbar. If the decay time of 0.004 second for the motion is assumed correct, then from equation (3) the stress is more nearly 13 kbar.

Since the motion was opposed by drag, the drag force is

$$F_d \sim v^n \tag{15}$$

and using $F_d = \sigma A$ where σ is the above calculated stress and A is the gauge plate frontal area, we can estimate the value of n at the initial condition,

$$n \sim \frac{\ell n\ \sigma A}{\ell n\ 270} = \frac{\ell n(145{,}000)(9.3 \times 10^{-2})(6.895 \times 10^{3})}{\ell n\ 270}$$

$$\underline{\sim}\ 3.3 \tag{16}$$

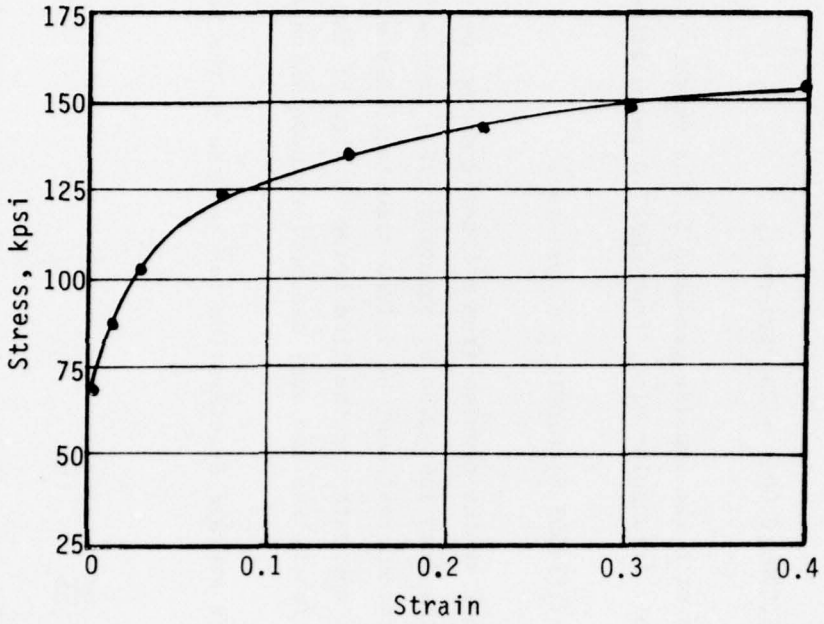

Figure 25. Stress-strain relation for 1045 steel, austempered at 600°C (Reference 15). This data is for uniaxial compression.

Thus,

$$F_d \sim v^{3.3} \tag{17}$$

which is approximately in agreement with the exponent of the velocity equation (11). In equation (16), the plate area is 9.3×10^{-2} m^2 and the other number is a conversion factor.

The dynamic motion discussed above occurring over a time of about 0.004 second can be looked upon as an impulse, approximately triangular in shape, so that

$$I_d \simeq \frac{1}{2} \sigma\tau = \frac{1}{2} (145{,}000)(0.004) = 290 \text{ psi-sec.} \tag{18}$$

This value is to be compared with the impulse produced by the shock. Since the shock profile is approximately triangular also, from CHART D calculations

$$I_s \simeq \frac{1}{2} P_s \tau_s = \frac{1}{2} (12)(14503.8)(0.001) = 87 \text{ psi-sec.} \tag{19}$$

We also attempted to look at the problem from a kinetic energy point of view. However, if we can believe the drag law given by equation (15), then a nonlinear differential equation is obtained that must be solved simultaneously with an energy equation. We abandoned this approach for the time being in view of the lack of evidence to support that approach, and the many assumptions upon which an answer would rest.

A simple estimate of the average deceleration can be made in the following manner:

$$\frac{dv}{dt} \simeq \frac{\Delta v}{\Delta t} = \frac{\Delta v}{\Delta x} \cdot \frac{\Delta x}{\Delta t} = \frac{(\Delta v)^2}{\Delta x} \tag{20}$$

Because it was assumed that $\Delta v = v_o - 0.2v_o = 0.8v_o = 0.8(270) = 216$ m/sec and from equation (13) $\Delta x = 0.36$m, then

$$\frac{(\Delta v)^2}{\Delta x} = \frac{(216)^2}{0.36}\left(\frac{1}{9.81}\right) \simeq 13{,}200 \text{ g's.}$$

The initial deceleration may have been much larger. As an approximation, we set

$$a = \frac{dv}{dt} \simeq \frac{v(x)}{\tau}$$

and using equations (11) and (12) gives

$$a = \frac{48.4(x+0.61)^{-3.48}}{0.0046(x+0.61)^{4.48}} = 10521.7(x+0.61)^{-7.96}$$

so that at $x = 0$

$$a = 10521.7(0.61)^{-7.96} \simeq 55{,}000 \text{ g's.}$$

In the absence of independent measurements, it is not possible to assign a confidence level to these values of deceleration.

SECTION VIII
SELF-CONTAINED ELECTRONIC PACKAGE EXPERIMENT

As mentioned in other sections of this report, we took the opportunity to install an integrated circuit in the T-5A field experiment. The objective was to determine component survivability under high pressures and high displacements. Although this experiment was not part of this contract, we enclose the results because they may be of general interest.

The package consisted of an integrated circuit (555 Timer), a mylar capacitor, and two carbon resistors. It was assembled as an astable multivibrator (oscillator). Also included in the package, but not electrically connected to the other components, was a 2N5450-NPN transistor.

The circuit was first wired to a circuit board, then encapsulated in an epoxy cylinder approximately 2 inches in length and 1-1/2 inches in diameter. The epoxy cylinder was then surrounded with paper towels and tape to form a ball approximately 3 inches in diameter. The ball was placed in a one-pound coffee can and filled with epoxy. The plastic coffee can lid was then taped in place. The completed coffee can was placed against the back of the driver wall beside the pressure gauges discussed in this report.

On recovery, the coffee can was found shredded with the epoxy cylinder, paper towels, and bits of tape intermingled with the metal. The epoxy cylinder had suffered a blow on one edge which caused the epoxy to fracture near that corner. The blow and the fracturing dented the mylar capacitor, shorting it out, and caused half of the wired connections to shear at the circuit board. Three solder joints also separated. The capacitor and sheared wires were the closest components to the corner which received the blow.

Upon rewiring the oscillator circuit, it worked perfectly, indicating that the 555 Timer survived. Placing the 2N5450 transistor on a curve tracer showed that it

too had survived. While the circuit as a whole did not survive, all but one of the components survived.

The conclusion is that an electronic circuit can easily survive a blast the magnitude of the Yuma T-5A test. We only need to use a better quality coffee can. If a section of 6-inch diameter steel pipe had been used instead of a coffee can, the circuit would not have experienced the damage discussed above.

SECTION IX
CONCLUSIONS

The conclusions presented below are based on the analysis given in this report. Although the analysis is somewhat speculative, particularly where it concerns the pressure cell deformation process, the conclusions regarding stress magnitudes could not be significantly improved by a more detailed elasto-plastic analysis of these gauges. No independent measurements were made in the vicinity of our gauge in T-5A so that no supporting evidence is available. Despite this, the conclusions that can be drawn from this experiment are:

- All gauges and hence the pressure cells were recovered with relative ease. However, the post-test conditions resulting from the complete destruction of the driver wall caused us some concern. The gauges were found in the crater fallback, some 8 feet back from their original position, in the same relative position to a vertical mid-plane and approximately 1 foot higher than their original grade level position. One gauge was found upright facing back and the other lying down facing up, indicating that tumbling must have occurred.
- The pressure cells held their static preloading pressure for 27 days: from the time of calibration in the laboratory until just before shot time. This point is significant because the pressure was applied to the samples via AgCl, a waxy material with a high creep. Had there been a pressure loss, it would have occurred by extrusion of AgCl from the pressure vessel cavity past the pistons. Initially, two cells exhibited small pressure losses which were later recovered due to cell temperature increase from the alluvium.
- Considering that the driving force pushing the gauges back must have been quite high, the gauge plates held up well showing only minor damage.
- Seven cells were installed in the field, four containing MOVs and three RbCl. Of these, two MOVs were recovered, two were destroyed, and all three RbCl samples were also recovered.

- The MOV samples were examined and found to have been deformed during the pressure cell deformation. One MOV voltage-current measurement indicates a shock pressure value of about 9 kbar, but very little confidence can be attached to this value in view of the lack of good transient pulse data obtained with MOVs to date. The second MOV exhibited a runaway current at 90 volts, indicating that internal cracking had occurred providing paths for current flow. Hence, this particular MOV was useless.*

- An examination of the RbCl samples showed no phase changes in any of them despite the large flow they experienced. Taking static strain data just before shot time and pressure sensing plunger and piston area ratios into consideration, an upper limit of about 12 kbar was placed as the detectable shock pressure. In the absence of a phase change, we conclude that the shock pressure must have been less than 12 kbar.

- In view of the one measurable MOV and the RbCl samples, we conclude that the shock pressure must have been between 9 and 12 kbar. The calculated value was 12 kbar. However, AFWL (Reference 12) indicated the detonation yield to have been lower than the expected calculated value, thereby giving some support to our findings.†

- The pressure cell bodies and internal components were deformed to the point where they could not be unscrewed for analysis. They were sawed lengthwise and opened for analysis. An analysis of the deformed components indicates that it is unlikely that it was produced by the hydrostatic pressure from the shock when it engulfed the pressure cell. It was most likely produced by the mass motion initiated after the passage of the shock. The gauge plates and pressure cells were thus driven into the alluvium at an initially high velocity which rapidly decayed. Crude calculations show this may have occurred over a distance of 30 to 40 cm from the initial position and in about 5 msec.

---

*GE—TEMPO has an on-going program to investigate MOV characteristics following a transient load.

†Mr. R. Bass at Sandia Laboratories was pleased with this conclusion since it confirmed the validity of his equation of state model for the CHART D calculations performed for us.

The motion raised the stress level in the cell to about 9 to 13 kbar, roughly the same order as the shock pressure. This kind of large displacement had not been expected on the basis of similar AFWL tests (T-3, for example).

- Pressure cell and associated component deformations can be overcome by a modification of the design. The principal modification involves using harder steel, shortening the piston and providing adequate stops to prevent destruction of the sample, and modifying the mount on the plate.

To sum up, on the basis of our findings to date, we believe that the experiment described in this report was not only successful but very useful.

SECTION X
RECOMMENDATIONS

The results described in this report represent the first high pressure gauge development test of this type conducted by GE-TEMPO. A considerable amount of useful information was acquired. The test was generally quite successful and the results indicate the basic approach of using solid state elements to measure high shock pressures is going in the right direction.

We recommend that several more of these types of field experiments be carried out to refine the concept and the design. We are currently conducting laboratory experiments to acquire a basic understanding of sensor material behavior at high transient stresses. This effort is intended to enable better control of measurement capability. These laboratory experiments would greatly benefit by participation in field experiments where the shock produced by explosives and the large displacements cannot be reproduced in the laboratory.

The Air Force Weapons Laboratory is planning a series of explosive tests for 1979, two of which appear to have the yield range needed for further prototype gauge development. We recommend that these two field experiments be used as an opportunity to refine the gauge design.

It is recommended that up to eight pressure cells in groups of four be emplaced in the crater region of the upcoming MISTY CASTLE event. The pressure cells would be mounted in magnetized heavy steel to maximize the recovery probability. When placed somewhat off-center from the charge in the crater region, their ejection trajectories can be predicted so that the search sector can be identified. Moreover, magnetic detector technology has advanced to the state where a ceramic magnetized disk the size of a penny can be detected beneath 8 feet of alluvium (Reference 14).

Finally, it is recommended that field experiments be continued so that the data produced can be used by calculators in the development of equations of state

for hydrocode predictions in alluvium and tuff and possibly other media. The experimental results reported here have elicited interest at Sandia Laboratories (Reference 2) because of their equation of state modeling for the CHART D computer code. Calculations of stress, particle velocity, and displacements are fairly straightforward and yield believable results at stresses below about 2 kbar and above about 50 kbar, but considerable difficulties are encountered within this stress range. Consequently, it would be useful to obtain data in this range (Reference 16).

Therefore, to sum up, it is recommended that two more field experiments (AFWL) be funded for continuing the development begun here, and that one additional set of gauges (8 pressure cells) be planned for installation within the crater region of MISTY CASTLE.

REFERENCES

1. Kotti, G.H., Capt., USAF, Letter to AFWL/DED-I with copies to General Electric Co.—TEMPO, August 21, 1978.

2. Bass, R., Sandia Laboratories, Albuquerque, NM, personal communication, August and November, 1978.

3. Samara, G.A. and W.L. Chrisman, "Study of Phase Transitions in Insulators by the Dielectric Constant Technique," in Accurate Characterization of the High-Pressure Environment, Ed. by E.C. Lloyd, NBS Special Publication No. 326, March 1971.

4. Voronov, F.F. and V.A. Goncharova, "Influence of Pressure up to 20 kbar on the Elastic Properties of Rubidium Chloride and Iodide," Soviet Physics JETP, Vol. 23, No. 5, 777-785, 1966.

5. Lacam, A. and J. Peyronneau, "Experimental Observation of Sudden High-Pressure Transitions in Alkali-Halides," VICHP: 2, Solid State Physics, 628-630 (1977).

6. Wong, J. and F.P. Bundy, "ZnO Varistors as Pressure Memory and Pressure Sensor," 77CRD263, General Electric Co.—Corporate Research and Development Center, Schenectady, NY, December 1977.

7. Cristescu, N., Dynamic Plasticity, North-Holland Publishing Company, Amsterdam, 1967.

8. Faires, V.M., Design of Machine Elements, 4th Edition, MacMillan, New York, 1966.

9. Hall, H.T., "High-Pressure Apparatus," in Progress in Very High Pressure Research, Ed. by F.P. Bundy, W.R. Hibbard, Jr., and H.M. Strong, John Wiley and Sons, Inc., New York, 1960.

10. Bryant, C., Air Force Weapons Laboratory, Kirtland AFB, NM, personal communication, September 13, 1978.

11. Levinson, L., General Electric Co.—Corporate Research and Development Center, Schenectady, NY, personal communication, October 1978.

12. Renick, J., Air Force Weapons Laboratory, Kirtland AFB, NM, personal communication, October 23, 1978.
13. Reid, C.N., Deformation Geometry for Materials Scientists, Pergamon Press, 1973.
14. Baum, N.P., CERF, University of New Mexico, personal communication, November 9, 1978.
15. Bridgman, P.W., Studies in Large Plastic Flow and Fracture, Harvard University Press, 1964.
16. Shunk, R.A., Electromechanical Systems of New Mexico, Inc., personal communication, November 7, 1978.
17. Ayala, J., Air Force Weapons Laboratory, Kirtland AFB, NM, personal communication, June 1978.
18. Letter to D.W. White, General Electric Co.-Corporate Research and Development, Schenectady, NY, informing him of our recent static measurements with medium voltage GE-MOV's, 11 December 1978.

DISTRIBUTION LIST

DEPARTMENT OF DEFENSE

Assistant to the Secretary of Defense
Atomic Energy
ATTN: Executive Assistant

Defense Advanced Rsch. Proj. Agency
ATTN: TIO

Defense Civil Preparedness Agency
ATTN: Asst. Dir. for Rsch., J. Buchanon

Defense Documentation Center
12 cy ATTN: DD

Defense Nuclear Agency
ATTN: DDST
2 cy ATTN: SPTD
4 cy ATTN: TITL
2 cy ATTN: SPSS

Field Command
Defense Nuclear Agency
ATTN: FCT
ATTN: FCPR
ATTN: FCTMOF
ATTN: FCTMEI

Field Command
Defense Nuclear Agency
Livermore Division
ATTN: FCPRL

NATO School (SHAPE)
ATTN: U.S. Documents Officer

Undersecretary of Defense for Rsch. & Engrg.
ATTN: Strategic & Space Systems (OS)

DEPARTMENT OF THE ARMY

Harry Diamond Laboratories
Department of the Army
ATTN: DELHD-N-P
ATTN: DELHD-I-TL

U.S. Army Ballistic Research Labs
ATTN: DRDAR-BLE, J. Keefer
ATTN: DRDAR-TSB-S
ATTN: DRDAR-BLV

U.S. Army Cold Region Res. Engr. Lab
ATTN: CRREL-EM

U.S. Army Engr. Waterways Exper. Station
ATTN: J. Ingram
ATTN: F. Hanes
ATTN: L. Ingram
ATTN: Library
ATTN: W. Flathau

U.S. Army Materiel Dev. & Readiness Cmd.
ATTN: DRXAM-TL

U.S. Army Nuclear & Chemical Agency
ATTN: Library

DEPARTMENT OF THE NAVY

David Taylor Naval Ship R & D Ctr.
ATTN: Code L42-3
ATTN: Code 1770

Naval Construction Battalion Center
Civil Engineering Laboratory
ATTN: Code L08A
ATTN: Code L51, R. Odello

Naval Facilities Engineering Command
ATTN: Code 09M22C

Naval Ship Engineering Center
ATTN: Code 09G3

Naval Surface Weapons Center
ATTN: Code F31

Office of Naval Research
ATTN: Code 715

DEPARTMENT OF THE AIR FORCE

Air Force Institute of Technology
Air University
ATTN: Library

Air Force Weapons Laboratory, AFSC
ATTN: DEX, J. Renick
ATTN: DE, M. Plamondon
ATTN: SUL
ATTN: DEX

Assistant Chief of Staff
Intelligence
Department of the Air Force
ATTN: INT

DEPARTMENT OF ENERGY

Department of Energy
Albuquerque Operations Office
ATTN: CTID

Department of Energy
Nevada Operations Office
ATTN: Mail & Records for Technical Library

DEPARTMENT OF ENERGY CONTRACTORS

Lawrence Livermore Laboratory
ATTN: Doc. Con. for Tech. Info. Dept. Lib.

Oak Ridge National Laboratory
Nuclear Division
X-10 Lab Records Division
ATTN: Civ. Def. Res. Proj., C. Kearny

Sandia Laboratories
ATTN: Doc. Con. for L. Vortman
ATTN: Doc. Con. for 3141
ATTN: Doc. Con. for A. Chabin

DEPARTMENT OF ENERGY CONTRACTORS (Continued)

Sandia Laboratories
Livermore Laboratory
ATTN: Doc. Con. for Library & Scty. Clas. Div.

OTHER GOVERNMENT AGENCIES

Central Intelligence Agency
ATTN: OSI/NED, J. Ingley

Department of the Interior
U.S. Geological Survey
ATTN: D. Roddy

DEPARTMENT OF DEFENSE CONTRACTORS

Acurex Corporation
ATTN: K. Triebes

Aerospace Corporation
ATTN: P. Mathur
ATTN: Technical Information Services

Agbabian Associates
ATTN: M. Agbabian

Artec Associates, Inc.
ATTN: D. Baum

BDM Corporation
ATTN: T. Neighbors
ATTN: Corporate Library

Boeing Company
ATTN: Aerospace Library
ATTN: E. Lempriere

California Research & Technology, Inc.
ATTN: K. Kreyenhagen

Civil Systems, Inc.
ATTN: J. Bratton

Develco, Inc.
ATTN: L. Rorden

Effects Technology, Inc.
ATTN: R. Wengler

EG&G Washington Analytical Services Center, Inc.
ATTN: Library

Electromechanical Sys. of New Mexico, Inc.
ATTN: R. Shunk

Eric H. Wang
Civil Engineering Rsch. Fac.
University of New Mexico
ATTN: N. Baum

General Electric Company-TEMPO
ATTN: J. Shoutens
ATTN: C. Hudson
ATTN: S. Senesac
ATTN: DASIAC

Geocenters, Inc.
ATTN: L. Isaacson

DEPARTMENT OF DEFENSE CONTRACTORS (Continued)

H-Tech Labs, Inc.
ATTN: B. Hartenbaum

IIT Research Institute
ATTN: Documents Library

University of Illinois
Consulting Services
ATTN: W. Hall
ATTN: N. Newmark

Jaycor
ATTN: H. Linnerud

Kaman Sciences Corporation
ATTN: D. Sachs
ATTN: Library

Merritt CASES, Inc.
ATTN: J. Merritt
ATTN: Library

Physics Applications, Inc.
ATTN: C. Vincent

Physics International Company
ATTN: F. Sauer/C. Godfrey
ATTN: Technical Library

R & D Associates
ATTN: J. Lewis
ATTN: C. MacDonald
ATTN: Technical Information Center

Science Applications, Inc.
ATTN: Technical Library

Science Applications, Inc.
ATTN: J. Dishon

Science Applications, Inc.
ATTN: B. Chambers, III

Science Applications, Inc.
ATTN: K. Sites

Southwest Research Institute
ATTN: A. Wenzel
ATTN: W. Baker

SRI International
ATTN: G. Abrahamson
ATTN: B. Gasten/P. De Carli

Systems, Science & Software, Inc.
ATTN: D. Grine
ATTN: Library

Terra Tek, Inc.
ATTN: S. Green

TRW Defense & Space Sys. Group
ATTN: Technical Information Center
2 cy ATTN: P. Dai

TRW Defense & Space Sys. Group
ATTN: E. Wong

DEPARTMENT OF DEFENSE CONTRACTORS (Continued)

Weidlinger Assoc., Consulting Engineers
ATTN: M. Baron

DEPARTMENT OF DEFENSE CONTRACTORS (Continued)

Weidlinger Assoc., Consulting Engineers
ATTN: J. Isenberg